

University of Kentucky

UKnowledge

University of Kentucky Master's Theses

Graduate School

2011

COMPACT VISION SYSTEM FOR MONITORING OF 3D WELD POOL SURFACE IN PIPE WELDING

Alexander Phillip Maroudis

University of Kentucky, amaroudis@uky.edu

[Right click to open a feedback form in a new tab to let us know how this document benefits you.](#)

Recommended Citation

Maroudis, Alexander Phillip, "COMPACT VISION SYSTEM FOR MONITORING OF 3D WELD POOL SURFACE IN PIPE WELDING" (2011). *University of Kentucky Master's Theses*. 655.
https://uknowledge.uky.edu/gradschool_theses/655

This Thesis is brought to you for free and open access by the Graduate School at UKnowledge. It has been accepted for inclusion in University of Kentucky Master's Theses by an authorized administrator of UKnowledge. For more information, please contact UKnowledge@lsv.uky.edu.

STUDENT AGREEMENT:

I represent that my thesis or dissertation and abstract are my original work. Proper attribution has been given to all outside sources. I understand that I am solely responsible for obtaining any needed copyright permissions. I have obtained and attached hereto needed written permission statements(s) from the owner(s) of each third-party copyrighted matter to be included in my work, allowing electronic distribution (if such use is not permitted by the fair use doctrine).

I hereby grant to The University of Kentucky and its agents the non-exclusive license to archive and make accessible my work in whole or in part in all forms of media, now or hereafter known. I agree that the document mentioned above may be made available immediately for worldwide access unless a preapproved embargo applies.

I retain all other ownership rights to the copyright of my work. I also retain the right to use in future works (such as articles or books) all or part of my work. I understand that I am free to register the copyright to my work.

REVIEW, APPROVAL AND ACCEPTANCE

The document mentioned above has been reviewed and accepted by the student's advisor, on behalf of the advisory committee, and by the Director of Graduate Studies (DGS), on behalf of the program; we verify that this is the final, approved version of the student's dissertation including all changes required by the advisory committee. The undersigned agree to abide by the statements above.

Alexander Phillip Maroudis, Student

Dr. Yuming Zhang, Major Professor

Dr. Zhi Chen, Director of Graduate Studies

COMPACT VISION SYSTEM
FOR MONITORING OF 3D WELD POOL SURFACE IN PIPE WELDING

THESIS

A thesis submitted in partial fulfillment of the
requirements for the degree of Master of Science in Electrical Engineering
in the College of Engineering
at the University of Kentucky

By

Alexander Phillip Maroudis

Lexington, Kentucky

Director: Dr. Yuming Zhang, Professor of Electrical Engineering

Lexington, Kentucky

2011

Copyright © Alexander Phillip Maroudis 2011

ABSTRACT OF THESIS

COMPACT VISION SYSTEM FOR MONITORING OF 3D WELD POOL SURFACE IN PIPE WELDING

Human welders have long been able to monitor a weld pool and adjust welding parameters accordingly. Automated welding robots can provide consistent movement during the welding process, but lack the ability to monitor the weld pool. A vision system attached to the welding robot could provide a way to monitor the weld pool substantially faster than a human being. Previous vision systems to monitor weld pool surfaces have been developed, but their uses are limited since the system is fixed in place. The compact vision system developed in this research attaches directly to the welding torch, which provides no limitations in weld pool monitoring. This system takes advantage of the specular surface of a molten weld pool by reflecting a pattern of laser beams from the weld pool surface. The deformation of the laser beam after it reflects from the weld pool surface can provide clues to the weld pool shape, and thus the penetration of the weld. Image processing techniques and geometric optics are used to reconstruct a weld pool surface shape based on the image captured of the deformed laser pattern.

KEYWORDS: GTAW Welding, Weld Pool, Image Processing, Vision System, Laser

Alexander Maroudis

12/05/2011

COMPACT VISION SYSTEM
FOR MONITORING OF 3D WELD POOL SURFACE IN PIPE WELDING

By
Alexander Phillip Maroudis

Dr. Yuming Zhang

Director of Thesis

Dr. Zhi Chen

Director of Graduate Studies

12/05/2011

TABLE OF CONTENTS

LIST OF FIGURES	v
1. Introduction	1
Basic Welding Operation	5
Objectives	7
Thesis Organization	7
Hardware Design	7
Software Design	8
2. Compact Vision System Design	9
Component Details	12
Light Sources	13
Design Parameters	15
3. Compact Vision System Experiments	20
Initial Images	22
Improvements to Compact Vision System Fixture	25
Experiments With Improved Compact Vision System Fixture	27
Final Version of Compact Vision System Fixture	30
Dot Matrix Images	33
4. Simulation	36
Optical Theory of System	39
Dot Matrix Simulations	42
5. Image Processing	47
Reflected Dot Extraction	49
Thresholding	51
Median Filtering	58
Morphological Operation	62
Centroid Calculation	63
Position Information Extraction	65
Row Position	65
Column Position	68

Reference Point Position	70
Dot Matrix Row-Column Position/UCS Conversion	71
6. Real Time Reconstruction of 3D Weld Pool Surface	73
Brief Summary of Weld Pool Reconstruction Algorithm	74
One Point Algorithm.....	78
Weld Pool Reconstruction Error	83
Real Time Reconstruction Results.....	84
Real Time Performance	86
7. Conclusion	89
Improvements/Future Work	90
References	92
Vita	93

LIST OF FIGURES

Figure 1.1, Legacy Welding Vision System.....	2
Figure 1.2, Compact Vision System.....	3
Figure 1.3, (a) Reflected Dot Matrix Pattern, (b) Reconstructed Weld Pool.....	4
Figure 1.4, Welding Power Supply With Gas Canisters	5
Figure 1.5, Torch on Orbital Pipe Welding Station	6
Figure 1.6, Weld Penetration Profiles.....	6
Figure 2.1, Original Compact Vision System	9
Figure 2.2, Weld Hat	10
Figure 2.3, Close Up of Compact Vision System Fixture, Front View	10
Figure 2.4, CVS Fixture Diagram: Front View.....	11
Figure 2.5, Point Grey Flea 3 Machine Vision Camera.....	13
Figure 2.6, (a) Laser with Optics, (b) Dot Matrix Pattern.....	13
Figure 2.7, Camera With Optical Interference Filter	15
Figure 2.8, Law of Reflection Diagram.....	15
Figure 2.9, Original Compact Vision System Fixture Concept	16
Figure 2.10, (a) Fixture Calibration, (b) Line Pattern on Imaging Plane	17
Figure 2.11, Reflection from (a) First Surface Mirror, (b) Second Surface Mirror.....	17
Figure 2.12, Reflection Diagram, (a) Second Surface Mirror, (b) First Surface Mirror	18
Figure 2.13, Laser Reflecting From Weld Pool.....	19
Figure 3.1, (a) Laser Line on Weld Pool, (b) Dot Matrix on Weld Pool.....	20
Figure 3.2, (a) Laser with Incorrect Orientation, (b) Laser with Correct Orientation.....	21
Figure 3.3, Reflection from (a) Concave Surface and (b) Convex Surface	22
Figure 3.4, Weld Pool Reflections from Single Line Laser Pattern	23
Figure 3.5, Extreme Convex Weld Pool Surface Reflection Using Line Pattern.....	24
Figure 3.6, Improved Compact Vision System Fixture Diagram	25
Figure 3.7, Improved Compact Vision System Fixture.....	26
Figure 3.8, (a) Front View of Imaging Plane, (b) Top View of Imaging Plane	26
Figure 3.9, Reflection of Laser Line Pattern from Weld Pool Using Improved Fixture.....	28
Figure 3.10, Gap Between Mirror and Imaging Plane	29
Figure 3.11, Unusable Area of Imaging Plane Due to Gap.....	30
Figure 3.12, Final Compact Vision System Fixture Diagram	31
Figure 3.13, Final Compact Vision System Fixture.....	31
Figure 3.14, (a) Final Fixture With Camera, (b) Top View of Final Fixture.....	32
Figure 3.15, Image Misaligned	33
Figure 3.16, Dot Matrix Images From Weld Pool Reflection	34
Figure 4.1, Fixture Showing UCS Axes.....	36
Figure 4.2, Image Plane Coordinate System	37

Figure 4.3, Universal Coordinate System Conversion.....	38
Figure 4.4, UCS Conversion Constants.....	38
Figure 4.5, Top View of CVS Fixture Showing Orientation of Imaging Plane.....	39
Figure 4.6, Incident Rays Originating from Laser.....	40
Figure 4.7, Equation of a Sphere.....	40
Figure 4.8, Point on Weld Pool Surface is a Function of 3 Variables.....	40
Figure 4.9, Point on a 3D Surface.....	40
Figure 4.10, Ray Diagram of Weld Pool Reflection.....	41
Figure 4.11, Simulation: Convex Weld Pool Surface.....	43
Figure 4.12, Image Plane in Convex Simulation (a) Before Distortion of Weld Pool, (b) After Distortion of Weld Pool	43
Figure 4.13, Simulation: Concave Weld Pool Surface.....	44
Figure 4.14, Image Plane in Concave Simulation (a) Before Distortion of Weld Pool, (b) After Distortion of Weld Pool	44
Figure 4.15, Column Corresponding Relationship (a) Sequential/Convex, (b) Inverse/Concave	45
Figure 4.16, Row Corresponding Relationship (a) Sequential/Convex, (b) Inverse/Concave	46
Figure 5.1, Image Processing Flowchart	48
Figure 5.2, Reflected Dot Extraction Flowchart.....	49
Figure 5.3, Sequence of Images for Reflected Dot Extraction.....	50
Figure 5.4, Threshold Equation.....	52
Figure 5.5, Original Greyscale Image Histogram.....	52
Figure 5.6, Threshold Value for Method 1 of Global Thresholding.....	53
Figure 5.7, Image After Global Thresholding, Method 1	54
Figure 5.8, Histogram Intensity Range for Method 2 of Global Thresholding	55
Figure 5.9, Global Threshold Value: Method 2.....	55
Figure 5.10, Image After Global Thresholding, Method 2	56
Figure 5.11, Block Thresholding Equations.....	57
Figure 5.12, Binary Image After Block Thresholding	58
Figure 5.13, Salt and Pepper Noise Model (Impulsive Noise)	59
Figure 5.14, Probability Graph for Salt and Pepper Noise.....	59
Figure 5.15, 3x3 Median Filter Window	60
Figure 5.16, Binary Image (a) Before Median Filter, (b) After Median Filter	61
Figure 5.17, Morphological Operation: Dilation.....	62
Figure 5.18, (a) Image Before Dilation, (b) Image After Dilation.....	63
Figure 5.19, Centroid Calculation	63
Figure 5.20, Original Greyscale Image with Center of Reflected Dots Shown, 80A	64

Figure 5.21, Original Greyscale Image with Center of Reflected Dots Shown, 125A	64
Figure 5.22, Position Information Extraction Flowchart.....	65
Figure 5.23, Row Position Flowchart	67
Figure 5.24, (a) Row Parsing Order and Angle Requirements, (b) Rearranged Rows in Increasing Order.....	68
Figure 5.25, Reference Column Identification	69
Figure 5.26, Reference Column	70
Figure 5.27, Reference Point Location.....	71
Figure 5.28, Dot Matrix Position of Reflected Dots	72
Figure 6.1, Weld Pool Reconstruction Data Path	74
Figure 6.2, 2D Slope Diagram.....	76
Figure 6.3, Row Slope Calculation Diagram	77
Figure 6.4, Column Slope Calculation Diagram.....	78
Figure 6.5, OPA Parse Directions	79
Figure 6.6, Flowchart of One Point Algorithm	80
Figure 6.7, Interpolated Weld Pool Surface (a) Side View, (b) Top View	81
Figure 6.8, 1-D B-Spline Cubic Interpolation Formula	81
Figure 6.9, Extrapolated Weld Pool Surface	82
Figure 6.10, (a) Centroids of Image at Start of Welding Process, (b) Flat Extrapolated Weld Pool.....	82
Figure 6.11, Error Between Actual and Computed Reflection Points	83
Figure 6.12, Consecutive Greyscale Images During Real Time Processing.....	85
Figure 6.13, Real Time Reconstructed Weld Pool Surfaces.....	86

1. Introduction

The object of this thesis is to develop a compact vision system to monitor a 3D weld pool surface during pipe welding. While reconstructing a weld pool surface is not new, the system that has been developed is novel since it is comprised of a compact fixture that can be mounted directly to the weld torch to monitor the weld pool surface in real time. This system could be applied to any type of automated welding system. Pipe welding was used in this research since its automation is accomplished by simply orbiting the weld torch around the pipe. The goal of the compact vision system is to monitor the welding process to improve the quality of the welds. The compact vision system that has been developed can enhance the effectiveness of industry welding robots by providing intelligence. Based on this system, future work can involve changing relevant parameters of the welding robot to further increase quality and speed.

Vision systems to reconstruct a weld pool surface have been previously researched at the University of Kentucky welding research lab [1]. The systems start with a laser that projects a pattern onto a specular weld pool surface. The molten metal of the weld pool provides a highly reflective surface which the laser pattern can reflect onto a flat imaging plane. Thus, the reflection of the laser pattern from the weld pool provides a way to reconstruct the weld pool deformation, which can indicate the quality of the weld. Cameras are used to record the weld pool reflections, and image processing algorithms are performed to determine the weld pool surface shape. The image processing code is written in MATLAB, so that the weld pool reflections can be

easily viewed in real time. Other methods for image processing in the future will include embedded systems and hardware assist via field programmable gate arrays (FPGA's).

Figure 1.1, Legacy Welding Vision System [1]

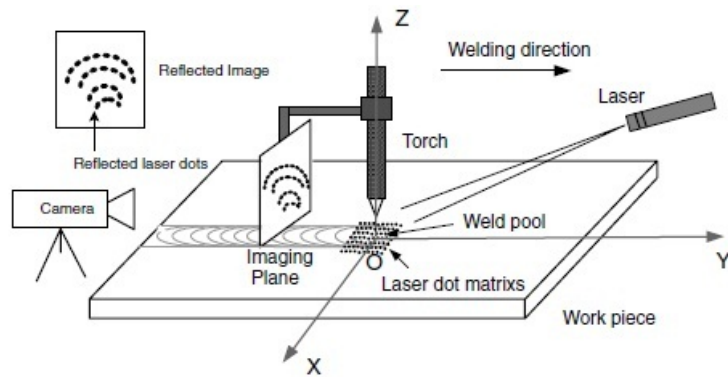


Figure 1.1 shows a system that has been used at the University of Kentucky welding research laboratory to reconstruct a weld pool surface. It is apparent from the figure that the laser and camera are not in close proximity to the torch and are fixed, not allowing the system to monitor the welding process over time. The three dimensional axes are visible in this figure and are used to determine the position of each reflected dot. The 3D position of each dot can then be input to the weld pool reconstruction algorithm that has previously been developed by students in the welding research laboratory.

Figure 1.2, Compact Vision System

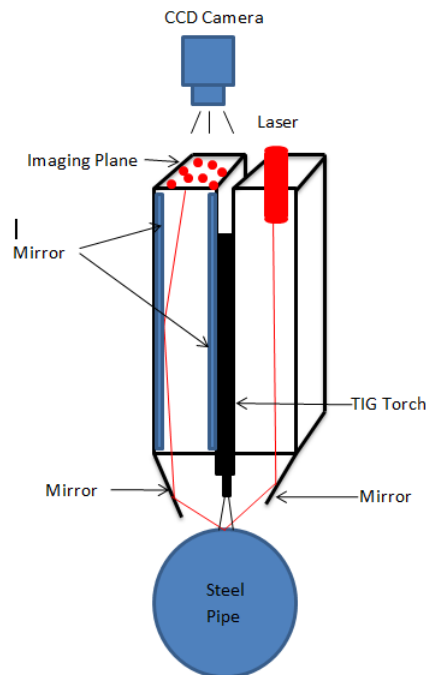
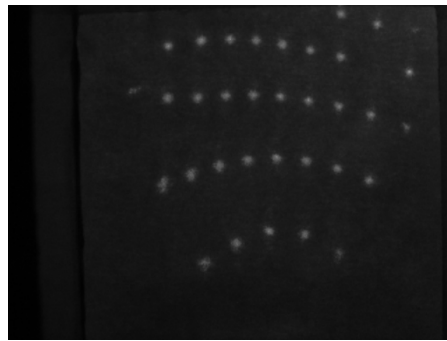


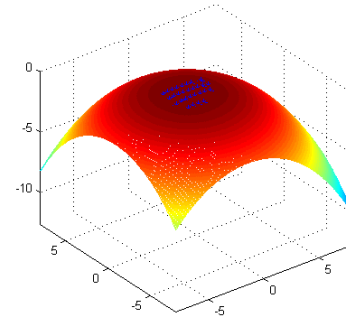
Figure 1.2 shows the original concept of the compact vision system weld torch fixture. The welding torch is sandwiched between two square aluminum pipes. In order to achieve a fixture that is compact, mirrors are used to redirect the laser. The imaging plane is now located at the top of the square pipe that receives the weld pool reflections. A camera above this pipe captures the reflected image for processing. The optics used on the laser for weld pool reconstruction will be a 19x19 dot matrix pattern. A simpler single line pattern will be initially used to prove the concept of the compact vision system. The goal of the image processing is to take a raw image from the camera, and determine the position information of each reflected dot. This position information includes the 3D coordinates of each dot as well as the dot matrix

row/column locations. This position information can then be input to the weld pool reconstruction algorithm.

Figure 1.3, (a) Reflected Dot Matrix Pattern, (b) Reconstructed Weld Pool



(a)



(b)

Figure 1.3 (a) shows the raw image from the camera of the dot matrix reflected from the weld pool, while figure 1.3 (b) shows the reconstructed weld pool surface. The curvature of the rows is proportionate to the degree of curvature of the weld pool surface. If the weld pool was more convex/concave, the curvature of the rows in the imaging plane would be exaggerated.

The final portion of this research is real time reconstruction of the weld pool surface. The position information of the reflected dots in the imaging plane will be calculated in real time, and the weld pool surface shape will be monitored during the welding process. This research is meant to prove the concept of the compact vision system, and MATLAB was chosen as the language to assist in the proof of concept. If the compact vision system is to be used commercially, the MATLAB software will need to be translated to run on an embedded system.

Basic Welding Operation

The welding process used in this research is gas tungsten arc welding (GTAW). The join between two metals in GTAW is accomplished by an arc between a tungsten electrode and the base material. The arc generated between the electrode and base material causes the base material to melt, thus joining the two metals. The weld area is protected from atmospheric contamination and oxidation by a shielding gas, usually argon. Equipment in a GTAW welding operation consists of a power supply, torch with tungsten electrode, arc igniter, and shielding gas. GTAW allows the operator greater control and precision than other welding process (GMAW,SMAW) because the operator has control of all the welding variables and a clear view of the arc [2].

Figure 1.4, Welding Power Supply With Gas Canisters

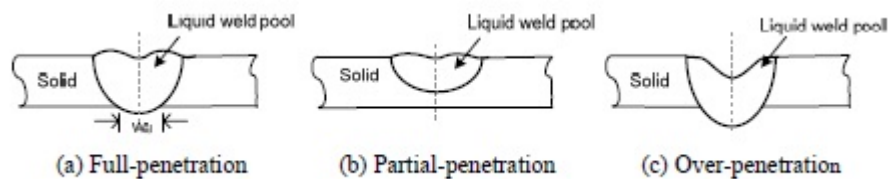


Figure 1.5, Torch on Orbital Pipe Welding Station



The variables in the welding process that can affect the quality of a weld bead include power supply current and voltage, flow of shielding gas, velocity of welding torch, and environmental conditions [2]. Penetration depth of the weld is used to gauge the quality of the welding process. It is this criterion that can be determined by the weld pool reconstruction algorithm. There are three types of penetration in a weld: full penetration, partial penetration, and over penetration [1].

Figure 1.6, Weld Penetration Profiles [2]



Full penetration is usually desired, and often required for critical welding applications [1]. Over penetration should be avoided since it can damage the material properties of the steel. Partial penetration can cause weaknesses in the weld seam, but is sometimes necessary to prevent burn through to the other side [1]. From figure 1.6, it is apparent that the shape of the weld pool changes depending on the weld penetration profile.

Thus, computational algorithms can be created to recreate the weld pool shape and determine the penetration of the weld.

Objectives

This research can be divided into four main objectives:

1. Build initial compact vision system fixture and acquire weld pool reflection images using a simple laser pattern.
2. Create a final prototype of compact vision system fixture and acquire weld pool reflection images using a dot matrix laser pattern.
3. Use image processing techniques to extract position information from images.
4. Achieve real time monitoring of 3D weld pool surface.

Thesis Organization

This research can be divided into two halves: hardware and software. The hardware half comprises of building the actual fixture and improving it to obtain the highest quality images possible. The software half involves processing these images to determine the weld pool shape and achieving real time monitoring of the weld pool.

Hardware Design

Chapter 2 describes the system design of the compact vision system fixture. The design of the initial fixture and the theory of its operation will be presented. Chapter 3 will present all of the experiments performed on the compact vision system fixture. Different techniques and methods to acquire the weld pool reflection images will be discussed. The progression of the compact vision system fixture from original concept

to working final prototype will be revealed. This chapter will cover all of the work necessary to obtain adequate images that can be processed by the software.

Software Design

Chapter 4 shows the MATLAB simulations of the compact vision system. The simulation will show the results of the laser reflecting from the weld pool onto the imaging plane. This chapter will establish the basis for the image processing chapter. Chapter 5 describes the image processing algorithms that transform the raw weld pool reflection images into binary images that can be used for weld pool reconstruction. Different binarization methods will be discussed, and the best method for this application will be determined. Algorithms for determining the 3D coordinates and row/column positions of the dots are presented. Chapter 6 presents the theory behind the weld pool reconstruction algorithm and how to input the results from the image processing step to reconstruct the weld pool. Also, discussion of using the compact vision system for real time reconstruction of the weld pool surface will occur.

Chapter 7 will present the conclusions of this research and discuss future improvements for the compact vision system.

2. Compact Vision System Design

The compact vision system (CVS) fixture will be used to reconstruct the shape of the weld pool surface, and determine if sufficient penetration has occurred. Images captured using this fixture can be used to monitor the welding process in real time.

Figure 2.1, Original Compact Vision System

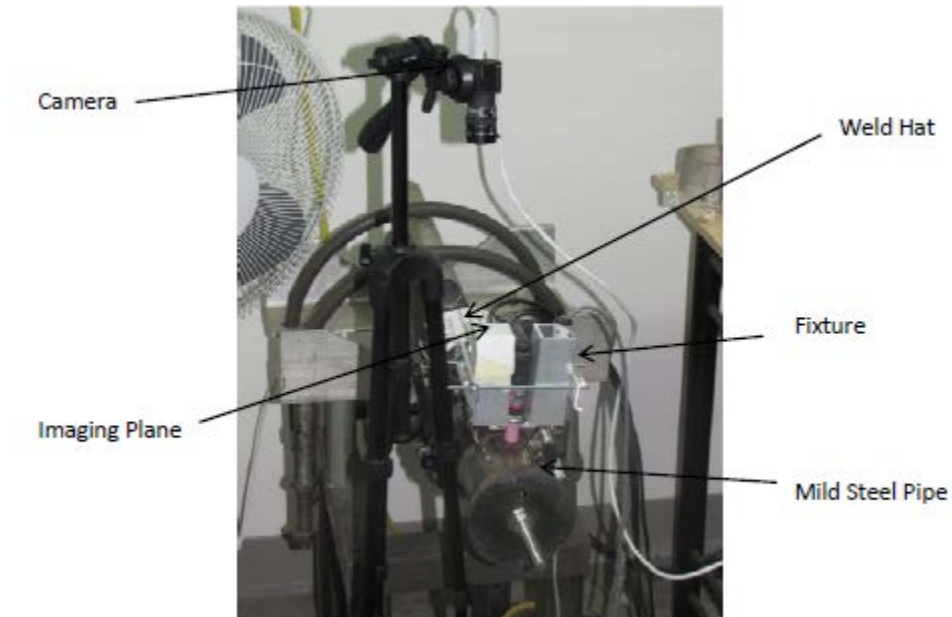


Figure 2.1 shows the CVS on an orbital pipe welding platform. The orbital platform has the pipe fixed, and a motor in the weld hat causes the torch to orbit the pipe. Two pipes can be inserted on the platform, and the torch can make one revolution around the pipes during welding to join the two pieces.

Figure 2.2, Weld Hat

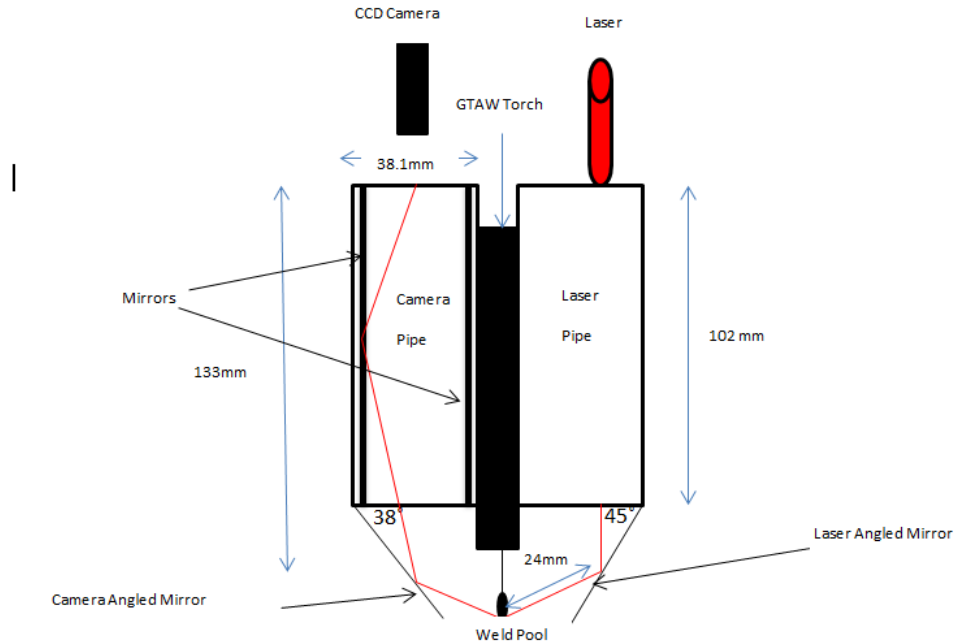


Figure 2.3, Close Up of Compact Vision System Fixture, Front View



Figure 2.3 shows that the GTAW torch is surrounded by the fixture, which sits atop the steel pipe during welding. The camera is above the imaging plane to capture the reflected images.

Figure 2.4, CVS Fixture Diagram: Front View



Figures 2.3 and 2.4 show the original design concept of the compact vision system fixture. The laser is mounted inside of an aluminum square pipe (laser pipe), which is aimed at an angled mirror (laser angled mirror) at the bottom of the tube. The beam is then reflected onto the weld pool, and the weld pool reflection is directed onto another angled mirror (camera angled mirror) on an adjacent aluminum square pipe (camera pipe). This camera pipe has mirrors on all four sides lining the inside, so that the laser can be reflected before it hits an imaging plane at the top. The goal is to achieve one reflection inside the camera tube to produce the clearest image possible. A camera is located above the imaging plane to capture the image. The theory is that the image will be deformed after it reflects from the weld pool, which will be either a concave or convex surface.

Component Details

The aluminum square tubes are 1.5 inches x 1.5 inches, and are 1/4 inch thick. The length of the tubes is approximately 4 inches. The power of the laser is 50 milliwatts, and the wavelength is 685 nanometers. The angled mirrors are attached to friction hinges via heavy duty adhesive tape. Friction hinges were used for fine angle adjustment, and to prevent the hinges from inadvertently moving during use. The friction hinges are attached to the tubes by a cold weld epoxy. Each angled mirror is approximately 1.5 inches x 1.5 inches. The GTAW torch is located between the laser and camera tubes. The tubes are held to the torch using aluminum rods and plates. The plates are tightened using nuts until the tubes are held securely in place. Memory foam was used to hold the laser in place inside the laser pipe. This allowed it to be adjusted easily, but also stay in place once adjustments were made. The mirrors inside the camera tube that reflect the image to the imaging plane are also attached via heavy duty adhesive tape.

The imaging plane consists of a flat sheet of plain white paper attached to a piece of glass to provide a smooth surface. The camera is external on a stand above the tube and is focused straight down on the imaging plane. The camera consists of a 1/3 "x 1/3" Sony CCD imaging sensor with a resolution of 640 x 480 pixels. It is a Point Grey Flea 3 machine vision camera, and comes with software to easily adjust the settings of the CCD. The camera transmits images to a computer via FireWire 800 interface.

Figure 2.5, Point Grey Flea 3 Machine Vision Camera [3]



A lens is needed to focus the light on the camera's CCD, and there are many lenses that are specifically designed for machine vision cameras. The lens used in this research is a Pentax 12mm F 1.2 lens.

Light Sources

There are two primary light sources contained in the compact vision system:

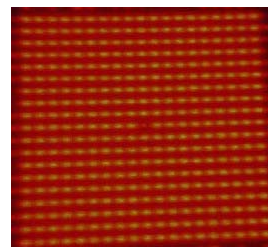
- 1) Weld arc light
- 2) Structured light laser.

The laser obtained for this research was a Coherent Systems 685 nm structured light laser. Different refractive lenses are available for this laser to generate the desired laser pattern. For this research, a single line and a 19x19 square dot matrix pattern is used

Figure 2.6, (a) Laser with Optics [4], (b) Dot Matrix Pattern



(a)



(b)

For the line pattern, the fan angle is 10 degrees. For the dot matrix pattern, the angle between the dots is 0.77 degrees. The laser also has adjustable focus, allowing for the diameter of the beam to expand and contract. Figure 2.6 (b) shows that the center dot of the dot matrix is absent. This absence of a center provides a reference point for all of the other dots. This reference point is crucial in determining what dots (column and row numbers) actually reflect from the specular weld pool surface, and is necessary for weld pool reconstruction.

The objective is to extract a clear image of the structured light laser pattern on the imaging plane after it reflects from the specular weld pool surface. Due to the nature of a laser, the intensity of the beam will not decrease much before it contacts the imaging plane. Conversely, the arc light intensity will decrease with the square of the distance [5]. Since this system is attached to the torch, the arc light will still be bright enough to interfere with the laser. The arc light contains wavelengths ranging from 340nm – 860nm, similar to white light [5]. Thus, an optical interference filter is required. The one chosen has a center wavelength of 685 nm (the same wavelength as the laser) and a bandwidth of 10 nm. The filter is placed before light enters the camera, to only pass the wavelength of the laser.

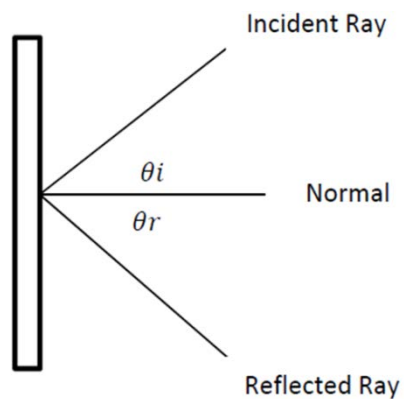
Figure 2.7, Camera With Optical Interference Filter



Design Parameters

The one equation that is used extensively in the design of the CVS fixture and weld pool reconstruction algorithm is the law of reflection: the angle with which the incident ray makes with the normal is equal to the angle with which the reflected ray makes with the normal.

Figure 2.8, Law of Reflection Diagram



This law of reflection is used to estimate the position and angle of the mirrors in the CVS fixture. Also, this law of reflection will be used to approximate the weld pool surface. Even though the weld pool is a spherical shape, the surface reconstruction is decomposed into smaller flat specular surfaces.

Figure 2.9, Original Compact Vision System Fixture Concept

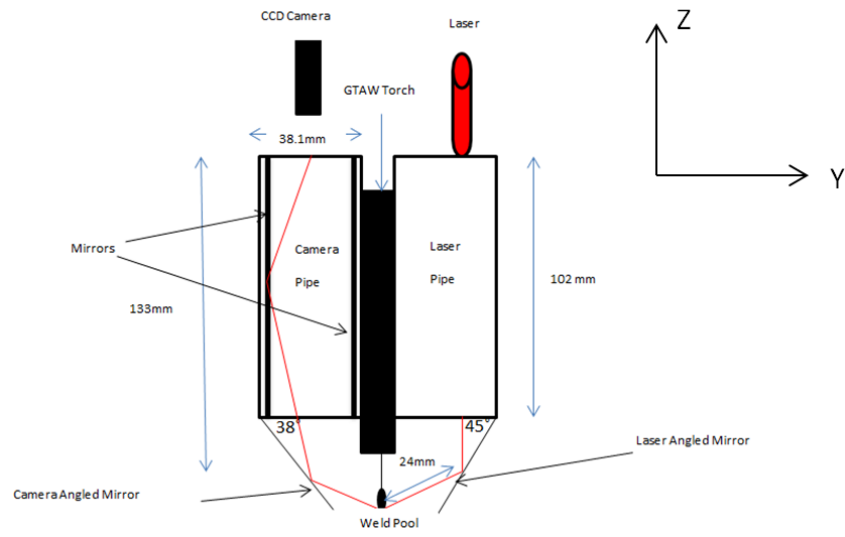
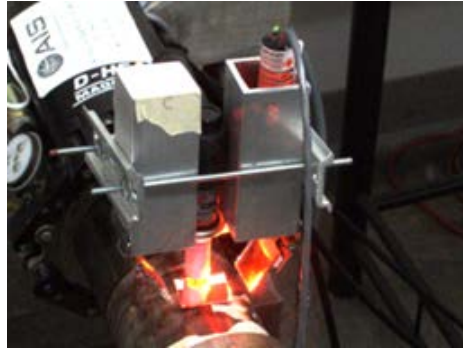


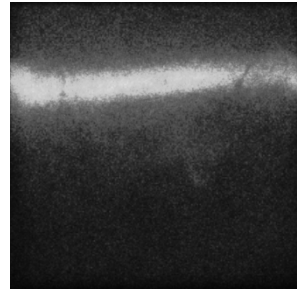
Figure 2.9 again shows the original concept for the compact vision system. As can be seen from the diagram, the easiest way to adjust this fixture is changing the angle of the mirrors that are connected to hinges at the bottom of the aluminum tubes. The laser angled mirror was positioned at 45 degrees, and the Y position of the laser was adjusted so that the laser would be incident onto the area below the welding torch tip. The law of reflection and basic trigonometry was used to estimate the angle of the camera angled mirror. The goal was for the laser to reflect from the mirrors lining the camera pipe halfway up, so that the reflected image would be centered in the imaging plane. Using this criterion, an angle of around 38 degrees was found best suited for the camera angled mirror.

A small mirror was placed to simulate the weld pool and make sure an image would appear in the plane. Using a mirror in place of the weld pool enables calibration of the fixture.

Figure 2.10, (a) Fixture Calibration, (b) Line Pattern on Imaging Plane



(a)



(b)

During the calibration phase of the original compact vision system fixture, it was discovered that the original mirrors chosen for this research were inadequate. A “ghosting” effect was noticeable due to the laser beam reflecting twice from the mirrors.

Figure 2.11, Reflection from (a) First Surface Mirror, (b) Second Surface Mirror



(a)

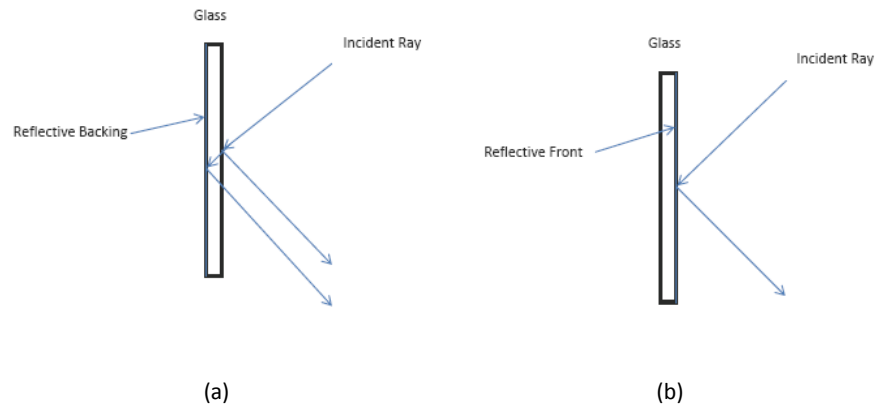


(b)

The original mirrors purchased were comprised of a highly reflective backing behind the glass. The reflective backing reflected most of the light, but a small amount was still reflected by the glass surface. This type of mirror is classified as a “second surface mirror”. To eliminate the “ghosting effect” from the multiple reflections, the original

mirrors were replaced with “first surface mirrors”, which have the reflective surface on top of the glass.

Figure 2.12, Reflection Diagram, (a) Second Surface Mirror, (b) First Surface Mirror



Having decided on design parameters for the original concept of the CVS fixture, the last detail is to find a suitable metal to be used as the pipe. No matter what laser optics pattern is used (line, dot matrix, etc), it is imperative that only the portion of the laser that is incident onto the weld pool is reflected. Stainless steel pipe can reflect a laser well due to its high reflective properties. This would cause a problem in the compact vision system during welding, because the laser pattern would be reflected from the specular weld pool surface, and from areas of the pipe outside the weld pool. These extra reflections contaminate the reflected image and makes weld pool reconstruction unobtainable. Thus, a mild steel pipe was chosen, which will only reflect the laser when it is incident onto the weld pool. Mild steel is the most common type of steel because it is relatively low cost and can be utilized in many applications [6]. It contains between 0.2 -0.3 % carbon and is neither brittle nor ductile. It is often used in

building large structures, and is optimal for welding [6]. The mild steel pipe allotted for this research has a thickness of 7.5mm.

Figure 2.13, Laser Reflecting From Weld Pool [1]

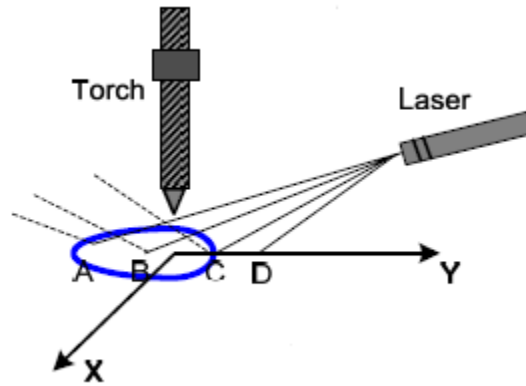


Figure 2.13 shows that points A, B, and C will be reflected from the weld pool when the pipe is composed of mild steel. Point D is outside the area of the weld pool, so a reflection does not occur.

The type of pipe that will be used and the parameters of the CVS fixture have been established. Experiments can now be performed to acquire reflected images of the laser from the weld pool. The design of the CVS fixture that has been established in this chapter is the original concept design. After experimentation, the design may need to be altered to achieve optimal results.

3. Compact Vision System Experiments

The experiments on the compact vision system will use a single line laser pattern to test out the functionality of the system. Once adequate images are obtained using the single line pattern, the dot matrix pattern will be introduced for image processing and weld pool reconstruction. The dot matrix pattern is much more suited for weld pool reconstruction because this pattern can be reflected from the entire surface of the weld pool. Starting with the single line pattern first will allow the functionality of the compact vision system to be verified quickly.

Figure 3.1, (a) Laser Line on Weld Pool, (b) Dot Matrix on Weld Pool



(a)



(b)

The line laser pattern must be incident onto the weld pool so that the line is transverse to the welding path direction.

Figure 3.2, (a) Laser with Incorrect Orientation, (b) Laser with Correct Orientation

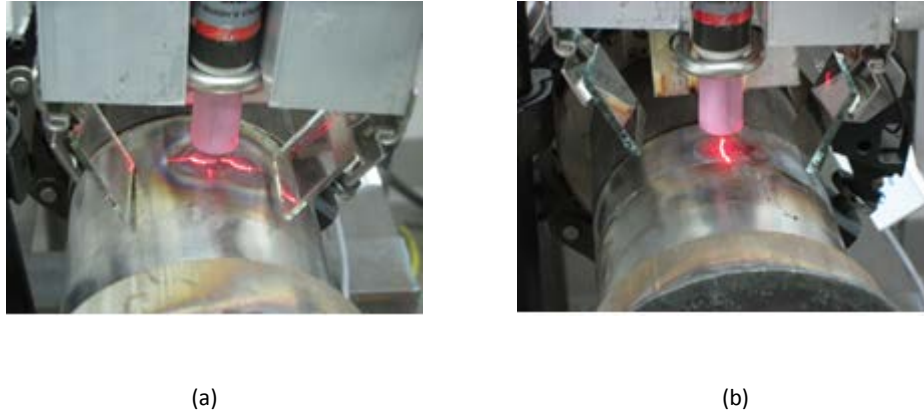


Figure 3.2 (b) shows the correct orientation of the line pattern. This correct orientation will guarantee that the reflected image's curvature changes with the weld pool surface shape. The orientation in figure 3.2 (a) will not produce a sufficiently curved image since the laser line will essentially remain straight regardless of the weld pool shape.

The Point Grey Research camera for this project has a variety of settings that adjusts many common camera parameters. Color imaging is not necessary since only the warping of the image is of concern, and would provide no extra benefit. Thus, greyscale imaging was used and an 8 bit grey level setting was chosen. The frame rate of the camera was set to the maximum value of 60 frames per second. During welding, the weld pool can oscillate at rates up to 100 Hz [7]. Using the maximum frame rate of the camera ensures that changes in the weld pool surface can be detected.

The welding current chosen for the beginning of the experiments was 80 amps. This amperage is considered to be nominal for welding mild steel pipes, and is a good starting value. The torch and fixture are connected to a "weld hat" that can be rotated around the pipe during welding. In this research, the torch will remain stationary due to

the limitations of the lens used on the camera. The focal length above the imaging plane for the lens (as seen in Figure 2.1) makes mounting to the fixture impractical.

Initial Images

To preview what the weld pool reflection images would look like, a simple experiment was performed using an ordinary spoon to simulate the weld pool surface. The spoon being placed upright represents a concave weld pool surface, and the spoon placed upside down represents a convex weld pool surface.

Figure 3.3, Reflection from (a) Concave Surface and (b) Convex Surface



(a)

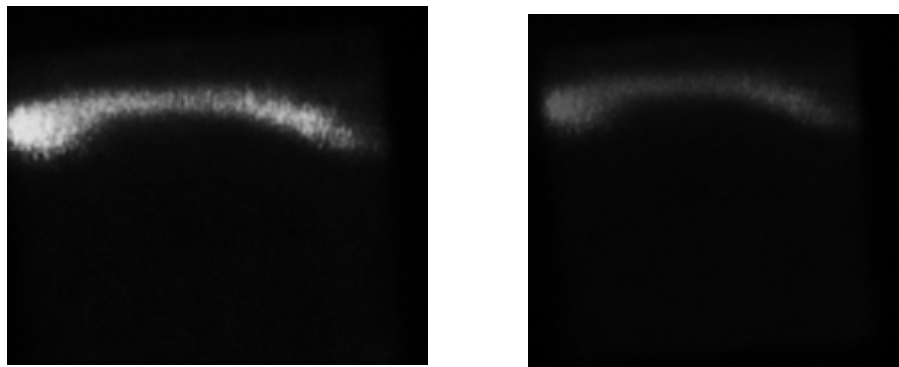


(b)

Similar shapes are obtained when reflecting a line from both types of weld pool surfaces. Intuitively, the more convex/concave the surface, the more pronounced the reflected curve will be.

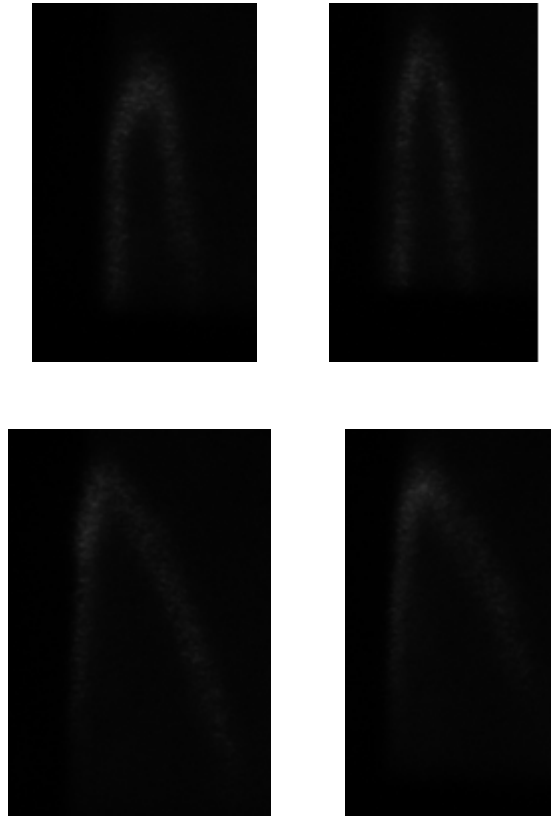
Now that the general shape of the laser reflecting from the weld pool surface has been established, results from welding experiments can be used as a comparison. After commencing welding, images were obtained from the single line structured laser reflected from the weld pool surface. The welding current was set to 80A and the tip of the electrode was 3 mm away from the surface of the pipe.

Figure 3.4, Weld Pool Reflections from Single Line Laser Pattern



The images in figure 3.4 are similar to the images obtained in figure 3.3. This proves the capability of the CVS fixture. These images do not exhibit much curvature, so a filler material was added to the weld pool area to create a large convex surface. Again, a welding current of 80A was used with the same electrode spacing to acquire images of a highly convex surface.

Figure 3.5, Extreme Convex Weld Pool Surface Reflection Using Line Pattern



The images in figure 3.5 are more curved, which reveals the extreme convex weld pool surface that was created from adding the filler material. Even though the shape is easily recognizable, the intensity and contrast of the image is poor. This is partly caused by a lack of laser intensity when the reflected beam makes contact with the imaging plane. When a mirror was used as a stand in for the weld pool surface during calibration, the reflected image was high in intensity and contrast. The weld pool is obviously not as reflective as a mirror, so the image suffers from a loss of intensity and focus. When the weld pool exhibits large fluctuations in shape, the path of the laser can significantly change, adding or subtracting distance to the path. What was a focused image at the start of the welding process is now partially out of focus due to the

variation of the laser path. Generally speaking, the path of the laser is too long. Decreasing the length of the laser path should improve the overall quality of the weld pool reflection images. Thus, adjustments to the compact vision system fixture are required.

Improvements to Compact Vision System Fixture

To minimize the path of the laser, the entire right side of the fixture was removed, including the aluminum pipe that housed the laser and the mirror that reflected it onto the weld pool. Instead, a mount was used that connected the laser directly to the welding torch. With this new mount, the laser is only centimeters away from the weld pool, increasing the intensity of the laser on the weld pool.

Figure 3.6, Improved Compact Vision System Fixture Diagram

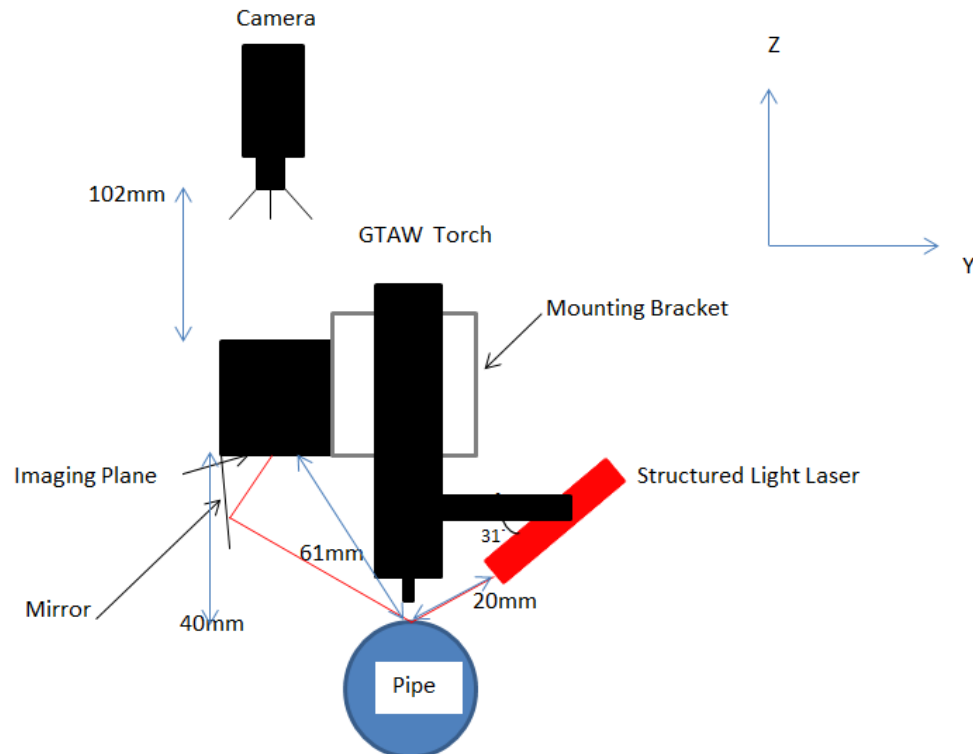
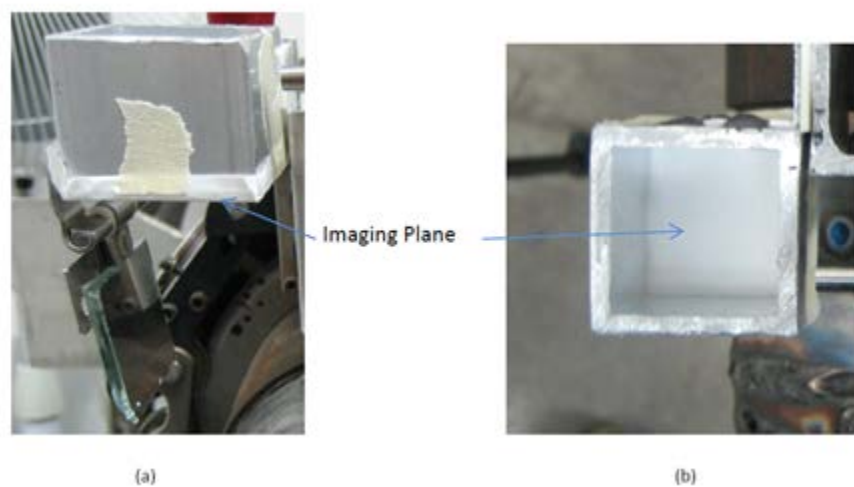


Figure 3.7, Improved Compact Vision System Fixture



To decrease the path of the laser after it has reflected from the weld pool, the imaging plane was changed from the top of the tube to the bottom. After the laser reflects from the weld pool, only one reflection from a mirror is now required to produce an image. The path of the laser has been reduced from a length of over 300 mm to 81 mm. These changes greatly simplify the fixture without sacrificing compactness or effectiveness.

Figure 3.8, (a) Front View of Imaging Plane, (b) Top View of Imaging Plane



Since the imaging plane is now on the bottom of the camera pipe, the height of it can be reduced to conserve weight. The reduced camera pipe was temporarily attached to the mounting bracket using heavy duty adhesive tape. The camera will now be looking down the remaining portion of the tube. Since the camera has a telephoto lens, the imaging plane will still be able to comprise most of the picture without the walls of the pipe interfering. The new V-mount that houses the laser does not have the ability for fine adjustment of its incident angle. Thus, experimental trials were performed to determine the angle of the laser, as well as the angle of the mirror. These values correspond to 31° and 85° respectively. Also, another variable that could affect the functionality and robustness of the fixture is the imaging plane's height above the pipe. More experimental trials reveal that the imaging plane should be 40 mm above the pipe to achieve acceptable images.

Experiments With Improved Compact Vision System Fixture

Welding experiments were performed with the improved CVS fixture starting with the single line laser pattern. The reflected images from the weld pool were recorded and showed improved contrast and intensity.

Figure 3.9, Reflection of Laser Line Pattern from Weld Pool Using Improved Fixture

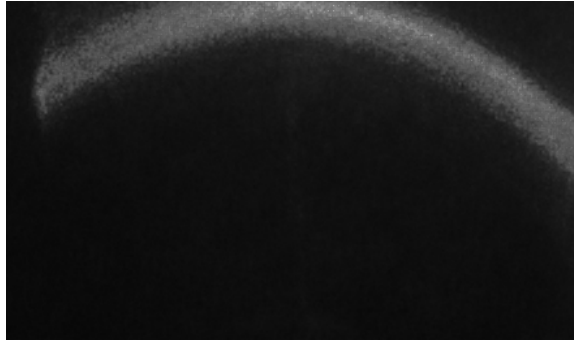
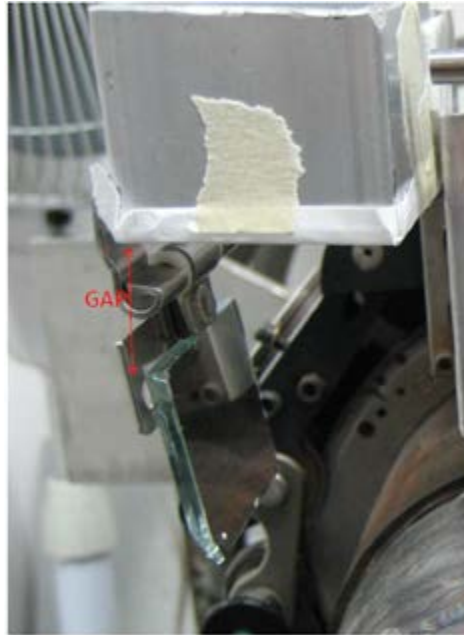


Figure 3.9 shows the laser line pattern reflected from the weld pool. This image shows a vast improvement in contrast and intensity compared to the images obtained from the original concept fixture. Now that the images from the weld pool reflections are satisfactory using the single line pattern, the 19x19 dot matrix pattern can be introduced. Since the dot matrix pattern will shine onto the entire weld pool surface, an accurate reconstruction of the weld pool can be realized.

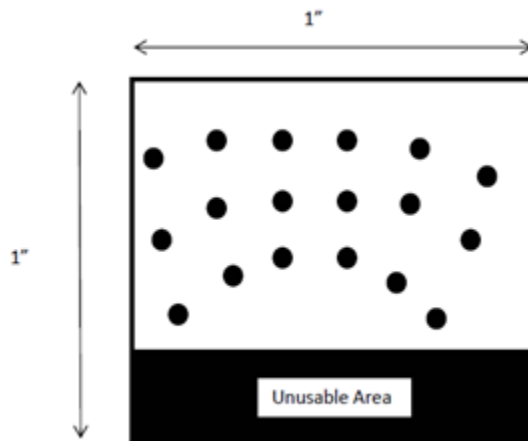
Since the laser line pattern only shone on a portion of the weld pool, there was a significant amount of margin during reflection from the mirror to achieve an acceptable image: the reflected line pattern could be located in many different portions of the imaging plane. For best results with the dot matrix pattern, the entire imaging plane should be available to display reflections from the weld pool surface. With this in mind, a flaw in the improved CVS fixture was discovered. Due to the nature of the hinges, there is a small gap between the top of the mirror and the imaging plane.

Figure 3.10, Gap Between Mirror and Imaging Plane



This gap makes a quarter of the imaging plane unusable. The nature of the CVS makes the imaging plane extremely small compared to legacy vision systems that were used for weld pool reconstruction. While legacy systems had imaging planes that are over 20 square inches [1], the imaging plane of the CVS must function with an area of only 1 square inch. Thus, it is critical that the CVS's entire imaging plane is usable for acceptable results.

Figure 3.11, Unusable Area of Imaging Plane Due to Gap



Final Version of Compact Vision System Fixture

To eliminate the gap between the mirror and imaging plane, the hinge could be repositioned to allow the weld pool reflections to be incident onto the entire area of the imaging plane. However, during analysis of this issue, a simpler solution was discovered. By lowering the imaging plane a few centimeters and increasing the angle of the laser slightly, the reflections from the weld pool were able to contact the imaging plane without using mirrors. This solution enables the entire imaging plane to be used, and greatly simplifies the design of the CVS fixture.

Figure 3.12, Final Compact Vision System Fixture Diagram

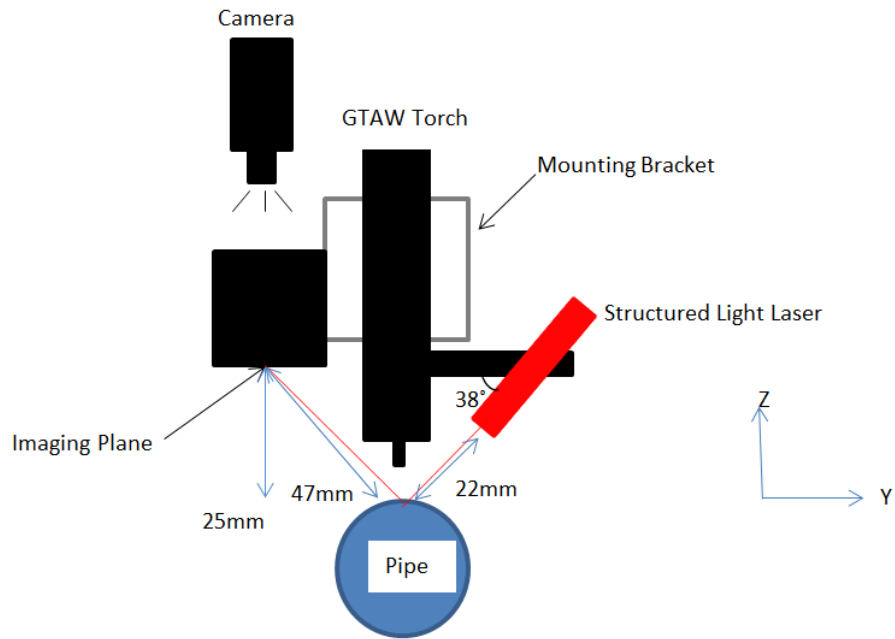


Figure 3.13, Final Compact Vision System Fixture



Figures 3.12 and 3.13 show the design of the final version of the CVS fixture. The mirror on the camera tube has been removed and the tube has been lowered to 25 mm above

the apex of the pipe, which allows the imaging plane to intercept the laser rays. The angle of the laser has slightly increased to 38° , while keeping the distance from the weld pool at around 22mm.

Figure 3.14, (a) Final Fixture With Camera, (b) Top View of Final Fixture



(a)



(b)

Figure 3.14 (a) shows the camera focused on the imaging plane. As previously stated, the lens prevents the camera from being closer to the imaging plane. Mounting the camera directly to the fixture is easily accomplished with a macro lens and will be mandatory when moving the welding torch around the pipe. Figure 3.14 (b) shows the fixture from the top view, which shows that the laser and imaging plane are nicely aligned along the Y axis. The goal is to have the laser pattern shine in the center of the imaging plane. Having the fixture physically aligned prevents the pattern from deviating much in the X direction.

Figure 3.15, Image Misaligned

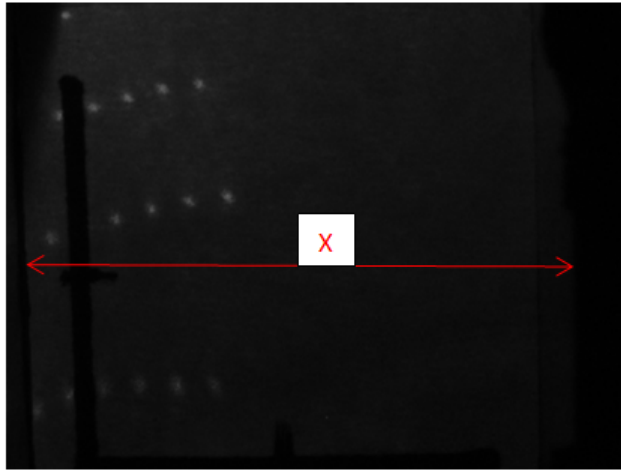
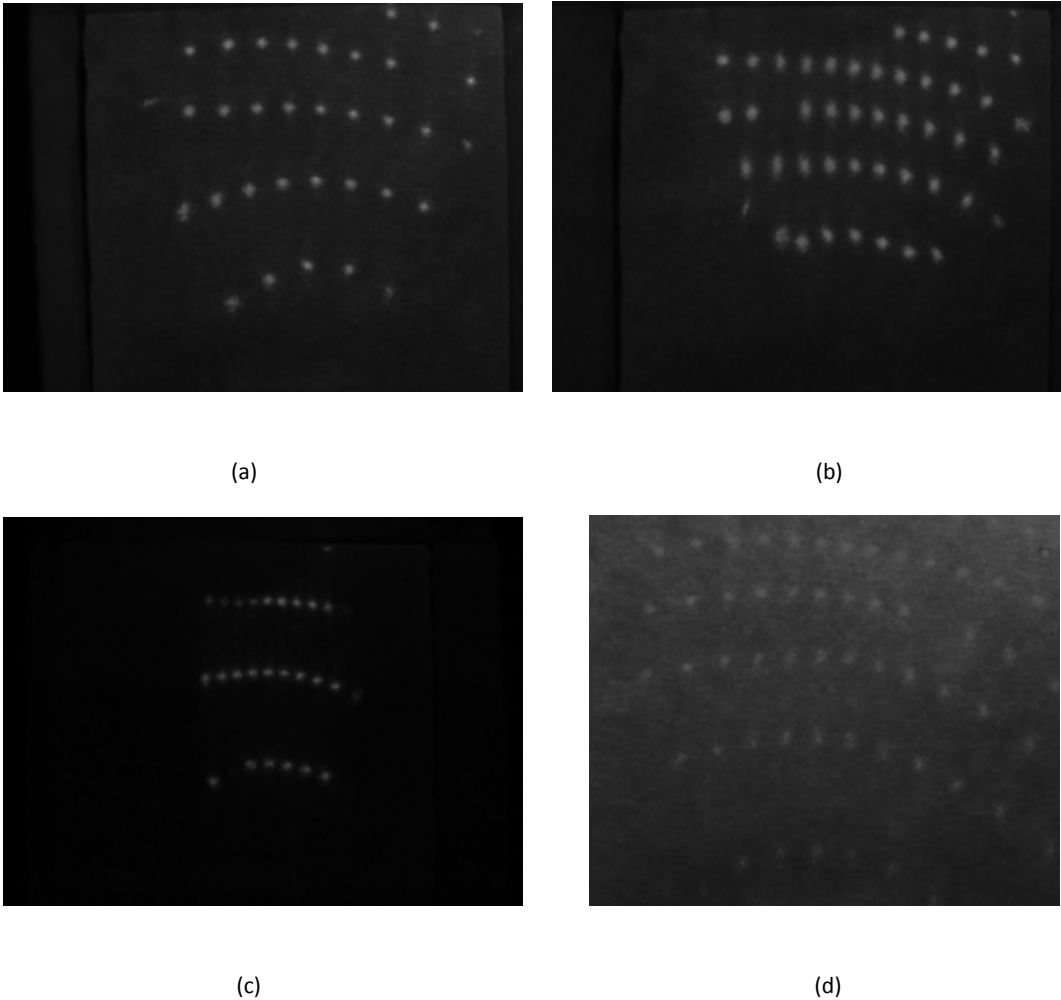


Figure 3.15 shows an example of the laser slightly misaligned and the dot matrix pattern appearing near the edge of the imaging plane. Misalignment causes the disappearance of some dots that would be captured if the laser was aligned properly. This would ultimately diminish information that could be used to reconstruct the weld pool surface. Since the imaging plane in this system is diminutive, it is critical to capture as many dots as possible to gain maximum information for weld pool reconstruction.

Dot Matrix Images

With the final version of the compact vision system fixture complete, images of the dot matrix being reflected from the weld pool can occur.

Figure 3.16, Dot Matrix Images From Weld Pool Reflection



Images obtained with the final version of the compact vision system fixture are in focus and display high levels of intensity. The welding current for the images in figure 3.16 (a) and (b) was a nominal value of 80A. Figure 3.16 (c) shows an image captured with a low welding current of 50A. Capturing images using a lower current is simpler since the arc will have minimal effect on the background and the dots will be easily extracted. Conversely, figure 3.16 (d) shows an image captured using a welding current of 120 A. This amperage is extremely high, and the bright background from the arc is apparent.

The dots are still visible, but extracting the dots is more difficult, since the contrast between the dots and background is minimal.

Removing the mirror and hinge assembly increases the compactness of the fixture and reduces the weight. The fixture is now very minimal in design and size, but still produces weld pool reflection images that can easily be used to determine the surface of the weld pool. The fixture has evolved from a device that reflects the laser from several mirrors, to one that uses no mirrors at all. This evolution has achieved the goal of building a compact fixture that captures excellent images of the laser pattern reflecting from the weld pool.

4. Simulation

A simulation in MATLAB was performed using the dot matrix pattern. This simulation shows the path of the dot matrix laser as it makes contact with the weld pool and reflects to the imaging plane. Before the simulation is run, parameters of the CVS must be known, including position information of the various components of the fixture. Thus, coordinate systems must be established.

To understand how the coordinates of the compact vision system are calculated, a universal coordinate system (UCS) needs to be established.

Figure 4.1, Fixture Showing UCS Axes

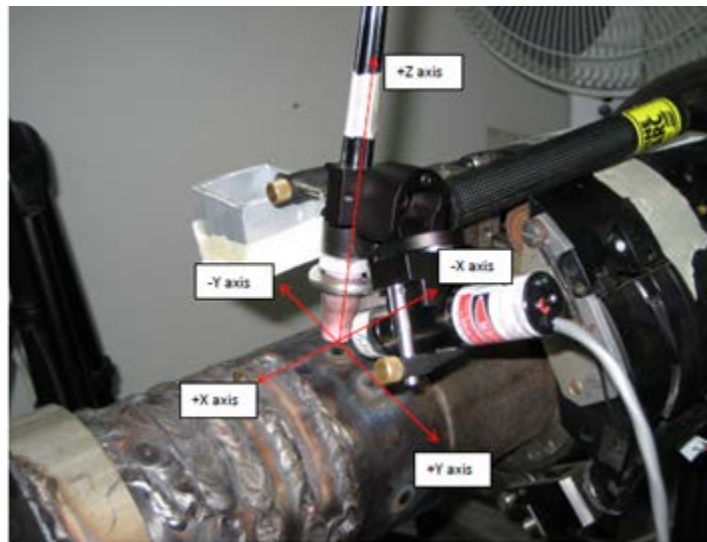
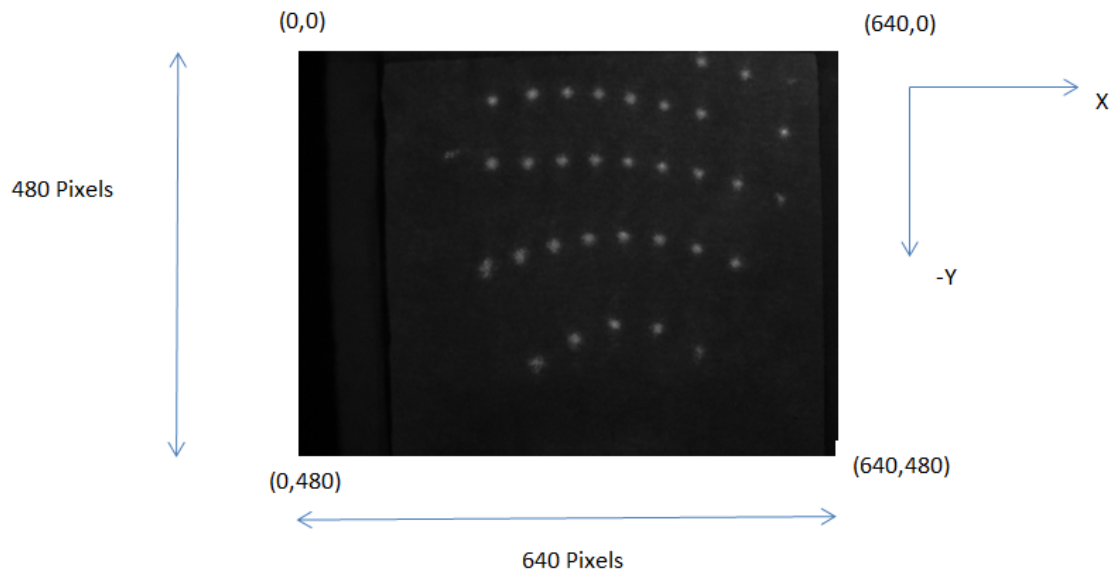


Figure 4.1 indicates how the axes are oriented in this system. The origin is located on the pipe right below the welding electrode tip. The positive Z axis moves up towards the torch, and the positive Y axis moves to the right. The positive X axis starts at the origin and extends away from the torch transverse to the Y axis. The units used to measure position information in the universal coordinate system are millimeters.

When processing images from the imaging plane, it is convenient to use a separate coordinate system to perform the image processing. This image coordinate system (ICS) will be used to calculate the centroids of the reflected dots in the imaging plane. Pixel values are used as the units in the ICS. The camera used in this system has a resolution of 640x480 pixels, and the camera is placed so that the imaging plane fits in the camera's entire field of view. The CCD sensor in the camera is parallel to the imaging plane.

Figure 4.2, Image Plane Coordinate System



For the ICS, the origin is the upper left hand corner of the image, while the bottom right hand corner represents (640,480). Since the imaging plane is square and the camera's aspect ratio is not, the sides of the tube will be partially visible. However, this has no effect on the processing of the image since the luminance of any dots on the sides of the tube will not be bright enough to be extracted in the image processing algorithm. These areas will be absorbed by the background during binarization of the image.

Once the position information of the reflected dots is calculated in the ICS, a transformation will convert the dots to the universal coordinate system for weld pool reconstruction. Since the imaging plane is fixed, the center of it has known universal coordinates. Also, to determine the size of each pixel, the top and bottom (Y direction) of the imaging plane is lined up with the camera's field of view. Since the distance is 1 inch from the top to the bottom of the imaging plane, each square pixel can be calculated to be 1/480 inch (0.053 mm) in length and width. The imaging plane coordinates can now be converted to universal coordinates.

Figure 4.3, Universal Coordinate System Conversion

$$\begin{cases} X_U = (X_I - 320) * 0.053 \\ Y_U = ((240 - Y_I) * 0.053) + Y_{Offset} \\ Z_U = Z_{Height} \end{cases}$$

These UCS conversion equations were determined by knowing the universal coordinates (units are still millimeters) of the center of the imaging plane, which is (0, -41, 23). With the universal coordinates of the imaging plane known, the constants for the universal coordinate conversion equations can be established.

Figure 4.4, UCS Conversion Constants

$$\begin{cases} Y_{Offset} = -41 \\ Z_{Height} = 23 \end{cases}$$

Figure 4.5, Top View of CVS Fixture Showing Orientation of Imaging Plane

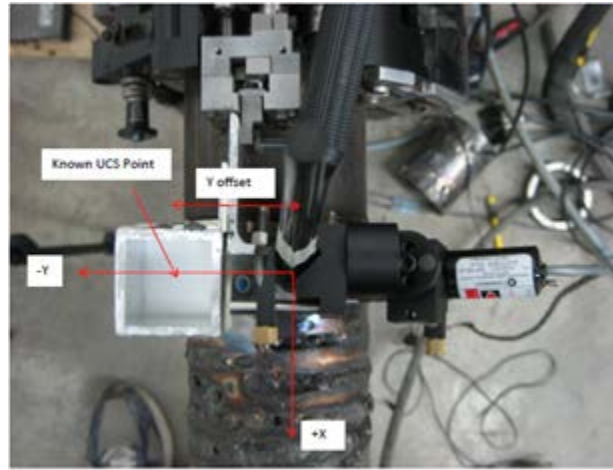


Figure 4.5 shows a top view of the CVS fixture. The orientation of the imaging plane's center with the pertinent axes is shown, and provides a visualization of the universal coordinate system conversion.

Optical Theory of System

Each dot that originates from the dot matrix laser can be represented by a vector. The properties of the laser needed to calculate the direction of this vector are fixed:

- 1) Universal coordinates of laser : (0,17.3,13.5)
- 2) Angle of laser : 38°
- 3) Interangle between dots : 0.77°

Figure 4.6, Incident Rays Originating from Laser

$$\begin{aligned}x_{i,j} &= x_0 + \bar{x}_{i,j} \\y_{i,j} &= y_0 + \bar{y}_{i,j} \\z_{i,j} &= z_0 + \bar{z}_{i,j}\end{aligned}$$

The incident laser ray originating from row i , column j of the dot matrix can be described by the equations in figure 4.6. Here, x_0 , y_0 , and z_0 represent the universal coordinates of the laser, while $(\bar{x}_{i,j}, \bar{y}_{i,j}, \bar{z}_{i,j})$ is the unit direction vector of each ray. To simulate a convex or concave surface, a sphere with a radius of r and a center at the origin was chosen.

Figure 4.7, Equation of a Sphere

$$x^2 + y^2 + (z - z_0)^2 = r^2$$

To simulate a convex surface, the top half of the sphere where $z > z_0$ is used, and for a concave surface, $z < z_0$ is used.

Figure 4.8, Point on Weld Pool Surface is a Function of 3 Variables

$$S = f(x, y, z)$$

Figure 4.8 shows that the surface of the weld pool and any surface will be a function of x , y , and z .

Figure 4.9, Point on a 3D Surface

$$P = (x_p, y_p, z_p)$$

Any point on the surface can be represented by the equation in figure 4.9.

The simulated weld pool surface was chosen to have a radius of 3 mm. Now that the weld pool's location and size is known, the intersection of the incident ray and weld pool can be computed to find a projected point. As stated, if the weld pool is a convex surface, the projected point will be the intersection of the incident ray and the sphere where $z > z_0$. If the weld pool is concave, the projected point will be the intersection of the incident ray and the sphere where $z < z_0$.

Figure 4.10, Ray Diagram of Weld Pool Reflection

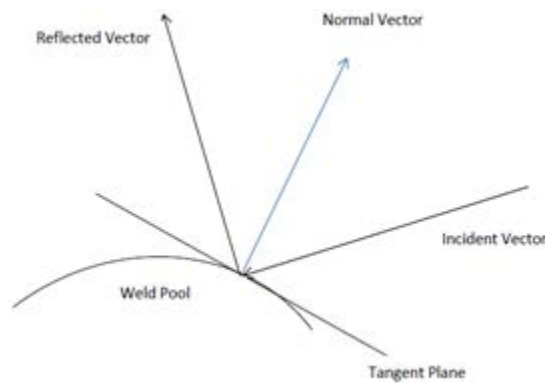


Figure 4.10 shows the geometric optics involved when reflecting a light ray from a weld pool surface. If the normal vector at the projected point on the surface and the incident vector are known, the reflected vector can be easily calculated using the law of reflection. In this case, the normal vector to the projected point is equivalent to the normal to the tangent plane of the surface at the projected point. Since the projected point is known, the normal can be easily calculated. Since the normal bisects the incident vector and reflected vector, the reflected vector can be computed when the normal is known. Once the reflected vector is known, the intersection of the imaging plane and reflected vector can be found to produce a dot in the imaging plane.

Dot Matrix Simulations

Now that coordinate systems have been established and the relevant geometric optics defined, a simulation can be performed. The base MATLAB code was obtained from the welding research laboratory at the University of Kentucky and was modified for the compact vision system. The simulation requires certain input parameters for operation:

- 1) Radius of Simulated Weld Pool : 3 mm
- 2) Laser Projection Angle : 38°
- 3) Interangle Between Laser Dots : 0.77°
- 4) Universal Coordinates of Laser : (0,17.3,13.5)
- 5) Image Plane Center Universal Coordinates : (0,-41,23)

The simulation was first run using a convex weld pool surface.

Figure 4.11, Simulation: Convex Weld Pool Surface

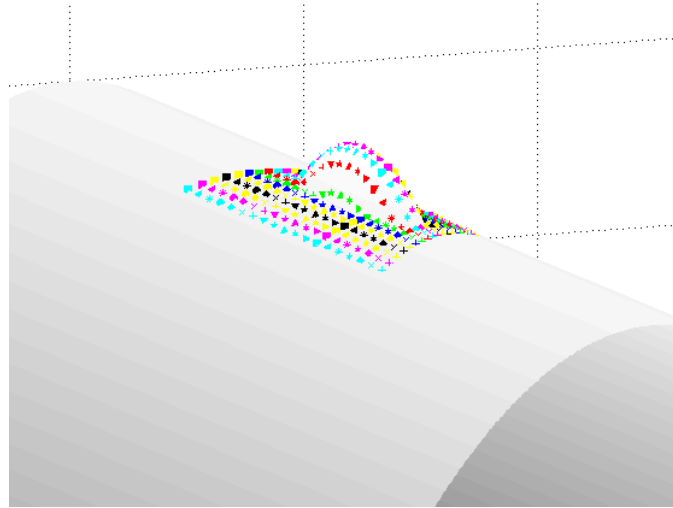


Figure 4.12, Image Plane in Convex Simulation (a) Before Distortion of Weld Pool, (b) After Distortion of Weld Pool

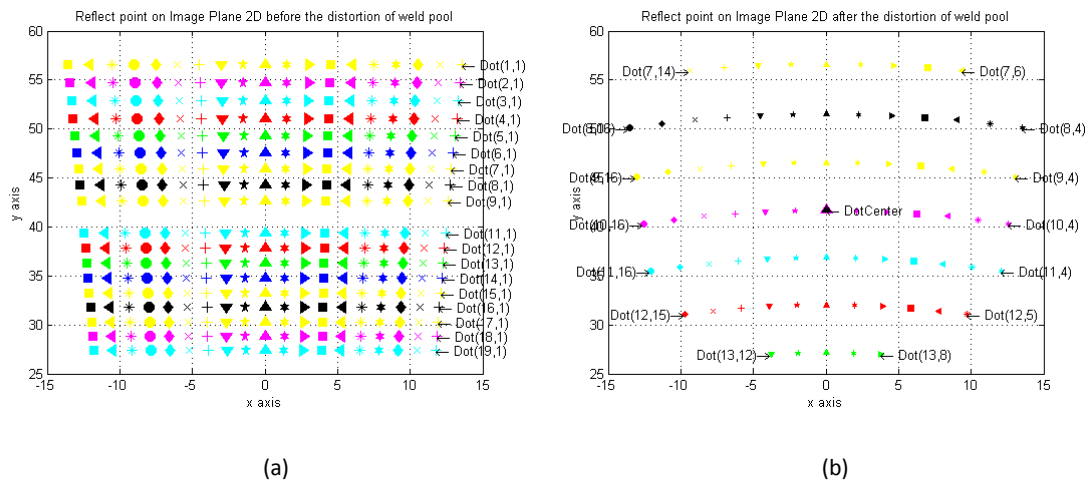


Figure 4.11 shows the dot matrix incident onto the convex weld pool. Figure 4.12 shows the image plane before and after weld pool distortion. Figure 4.12 (a) shows the dot matrix reflection from a flat surface; while figure 4.12 (b) shows the curvature of the dot matrix rows after it has been reflected from the weld pool. It is important to note that

the row and column positions are aligned with the non-distorted image. They exhibit a sequential relationship: the rows increase from top to bottom, while the columns increase from right to left for both the distorted and non-distorted images.

Figure 4.13, Simulation: Concave Weld Pool Surface

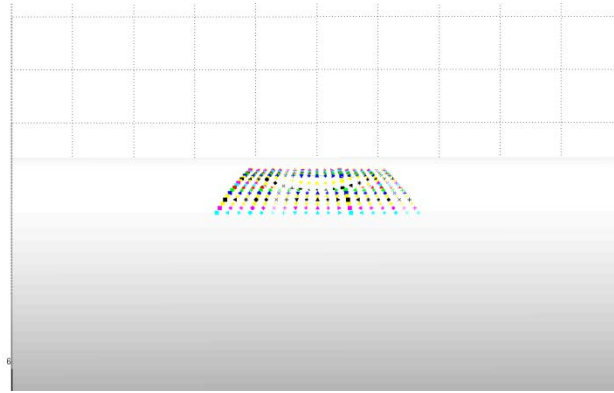


Figure 4.14, Image Plane in Concave Simulation (a) Before Distortion of Weld Pool, (b) After Distortion of Weld Pool

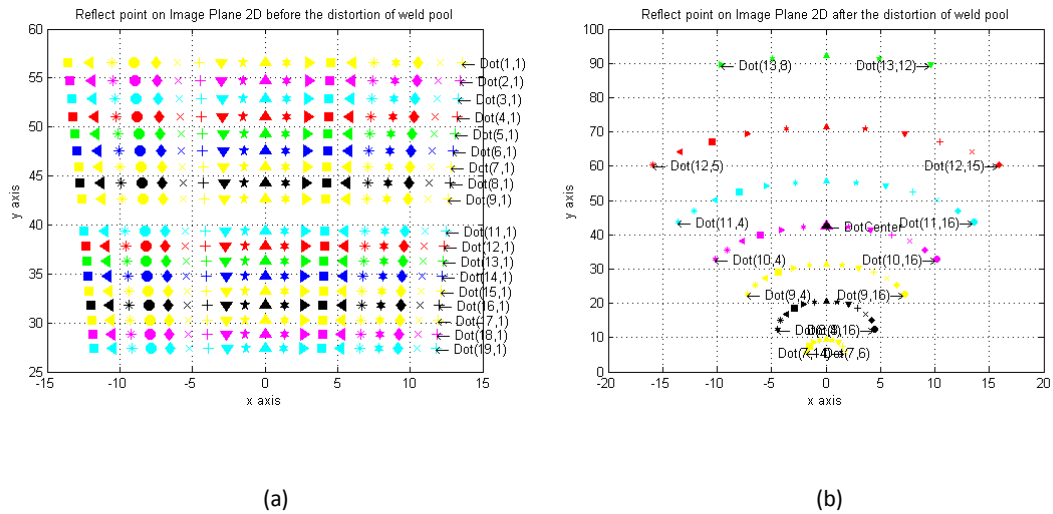


Figure 4.13 shows the dot matrix incident onto a concave weld pool surface. Similar to the convex simulation, figure 4.14 shows the image plane before and after weld pool distortion. For the concave surface, the rows and columns do not align like the

reflections from the convex surface: they exhibit an inverse relationship. Looking at figure 4.14(a), the rows increase from top to bottom, and the columns increase from right to left. Figure 4.14 (b) shows the opposite orientation for the dot matrix reflections from the concave surface: rows increase bottom to top and columns increase left to right.

Since the curvature of images from a convex and concave weld pool surface can be very similar, the relationship of the row and column positions can reveal the weld pool shape.

Figure 4.15, Column Corresponding Relationship (a) Sequential/Convex, (b) Inverse/Concave

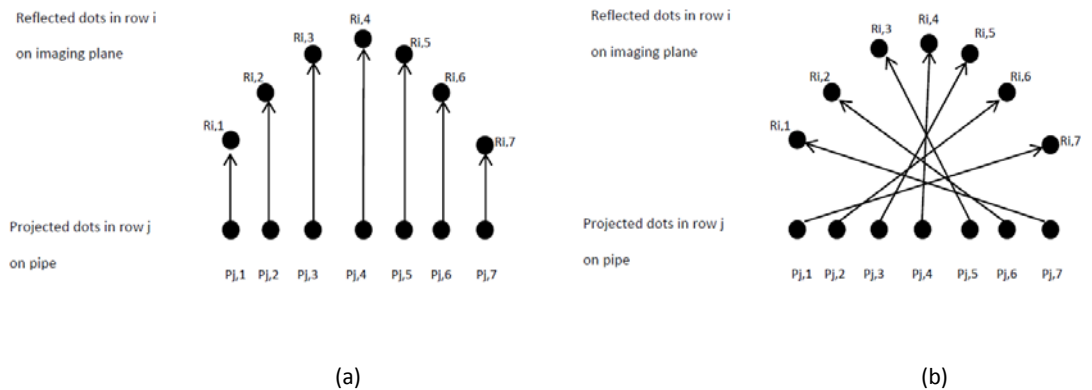
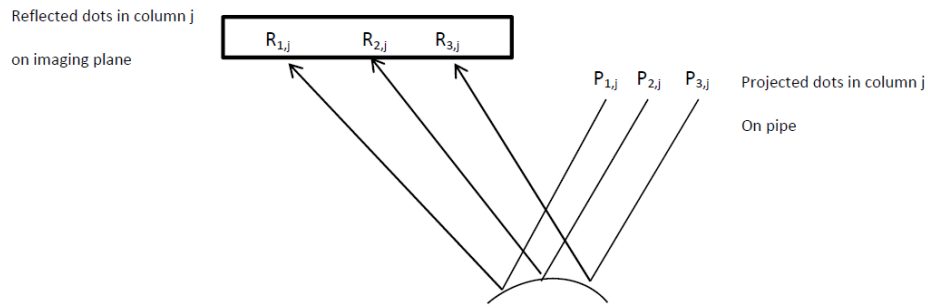
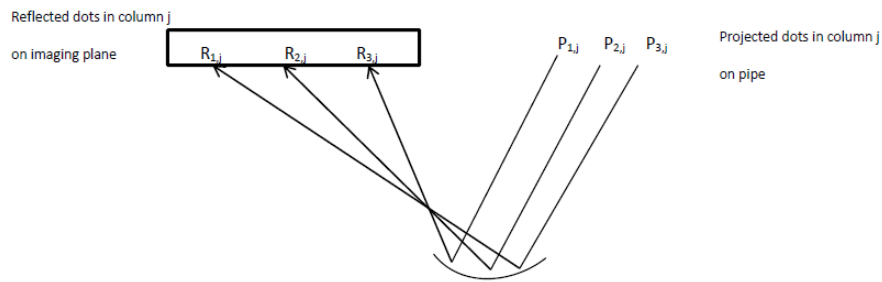


Figure 4.15 shows the column relationship between the projected and reflected dots. As discussed in the simulation, a convex weld pool surface will exhibit a sequential relationship and a concave surface will exhibit an inverse relationship.

Figure 4.16, Row Corresponding Relationship (a) Sequential/Convex, (b) Inverse/Concave



(a)



(b)

The same relationship applies to the rows, as figure 4.16 exhibits. A third relationship can also occur, which is disordered: no logical relationship can be found between the rows/columns of the projected and reflected patterns. This would indicate a weld pool with an irregular surface.

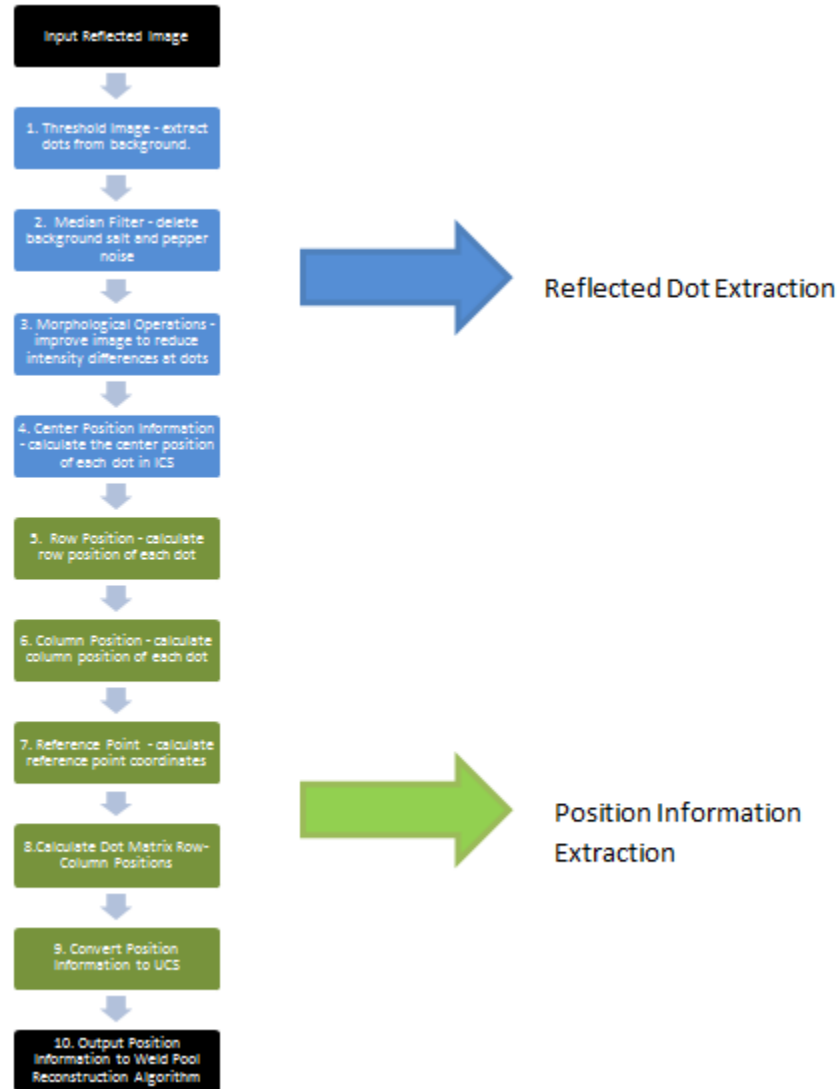
For this research, the weld pool shapes will be assumed convex. This is because the pipe being used is extremely thick, and the nominal amperage during experiments will only produce a convex surface. Hence, the weld pool reconstruction can be simplified since calculating the row-column relationships is not necessary.

5. Image Processing

Image processing is a field that is used in numerous engineering disciplines and is an essential tool of machine vision systems. Various image segmentation methods will be applied to the dot matrix reflection images to determine which method best converts the grey scale image to a binary image. These methods include thresholding, filtering, morphological operations, and pattern recognition. These methods will assist in calculating position information of the dots to be input to the weld pool reconstruction algorithm.

Figure 5.1 shows the complete flowchart for the image processing portion of this research. The blue section of the flowchart details the reflected dot extraction steps. The goal of this half of the flowchart is to obtain the center position information of the reflected dots. The green section of the flowchart details the position information extraction steps. The goal of this part of the flowchart is to extract the dot matrix row-column positions and reference point position. The reference point and centroid positions will then be converted to UCS for input to the weld pool reconstruction algorithm. Each of the steps in the flowchart will be explained in detail.

Figure 5.1, Image Processing Flowchart



Reflected Dot Extraction

The reflected dot extraction portion consists of 4 image processing operations on the original grey level image of the reflected dots.

Figure 5.2, Reflected Dot Extraction Flowchart

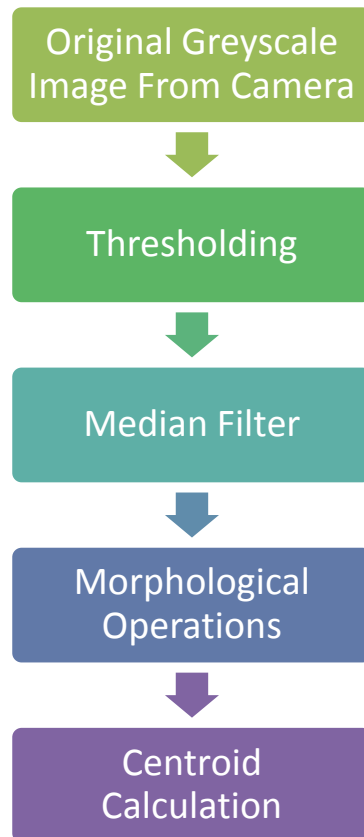


Figure 5.3 shows the image during each step of the flowchart from the previous figure.

Figure 5.3, Sequence of Images for Reflected Dot Extraction

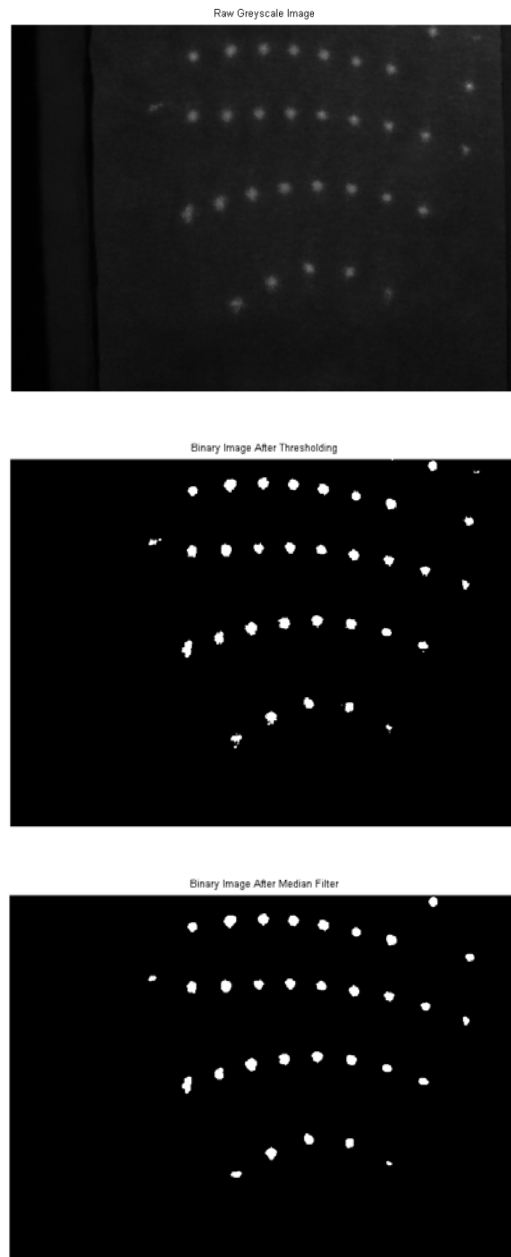
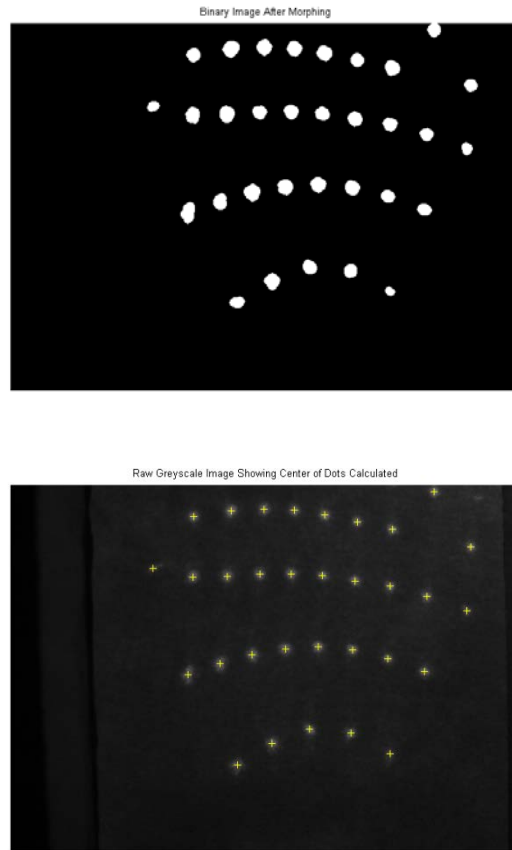


Figure 5.3 (continued), Sequence of Images for Reflected Dot Extraction



Thresholding

Thresholding is the process of taking a greyscale (or color) image as an input, and outputting a binary image [8]. The parameter that is used for thresholding is pixel intensity. The input image is parsed, pixel by pixel, and each pixel is compared to a threshold. If the pixel intensity is greater than or equal to the threshold, the corresponding pixel in the output image is a '1' (or white). If the input pixel is less than the threshold, the corresponding pixel in the output image is a '0' (or black). In the compact vision system, 8 bit greyscale images are used, so a '1' in the image after thresholding represents an intensity level of 255, while a '0' represents an intensity level of 0.

Figure 5.4, Threshold Equation

$$\begin{cases} f[m,n]_{output} = 1 \rightarrow f[m,n]_{input} \geq Threshold \\ f[m,n]_{output} = 0 \rightarrow f[m,n]_{input} < Threshold \end{cases}$$

Figure 5.4 summarizes the principle of thresholding, with $f[m,n]$ representing a pixel at row m , column n in the image. Two different methods of thresholding were performed to find the best suited method for this research: global thresholding and adaptive thresholding.

Global Thresholding

Global thresholding uses a fixed threshold for every pixel in the image. Thus, it is critical that the input image's histogram has sufficiently separated peaks to be able to separate the desired subject from the background [8]. In global thresholding, *Threshold* from figure 5.4 will be fixed.

Figure 5.5, Original Greyscale Image Histogram

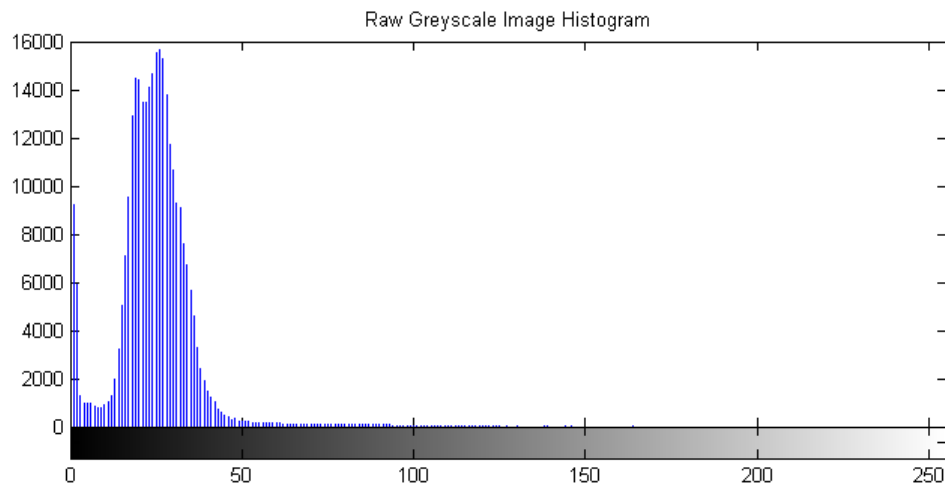
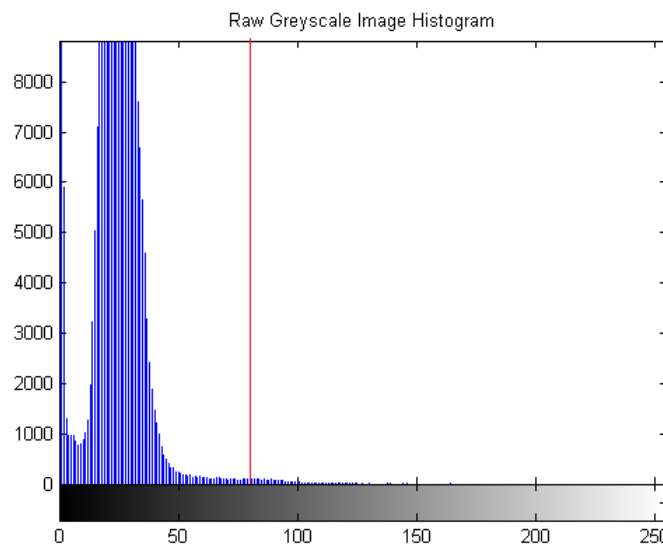


Figure 5.5 shows a histogram for the original greyscale image. The Y-axis represents “number of pixels”, while the X-axis represents “intensity value”. Two different

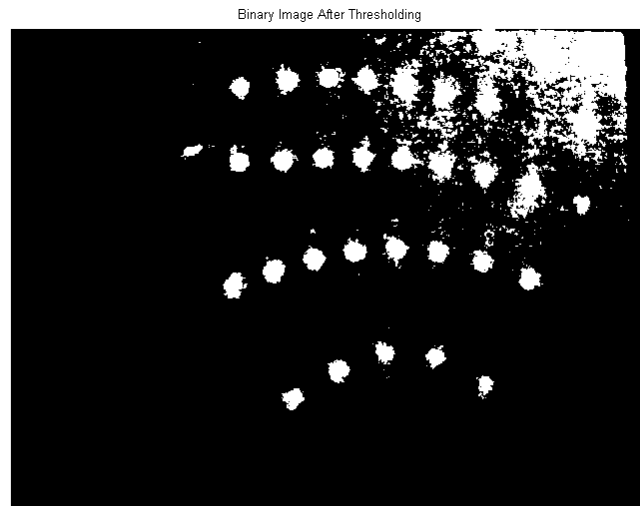
methods of global thresholding were attempted. Method 1 used a single value from the histogram for the threshold value, while method 2 used a range of intensity values in the histogram to calculate an average. It is apparent that the majority of the image is composed of dark regions, since the majority of the pixels have a grey level of 50 or less. The pixels with high intensity levels, represented by the reflected dots, are very small in numbers compared to the background pixels. Nevertheless, a global threshold attempt was performed.

Figure 5.6, Threshold Value for Method 1 of Global Thresholding



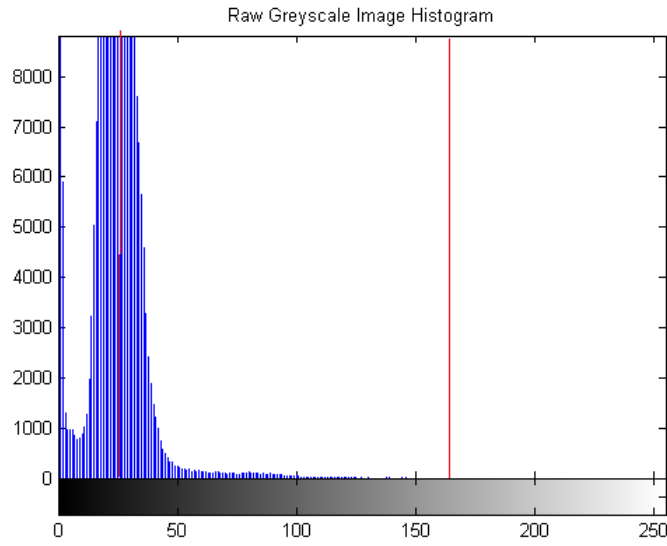
To determine a threshold value in this first method of global thresholding, the highest peak at the tail end of the histogram was calculated (shown by the red line in figure 5.6). The intensity levels of the reflected dots will have the highest intensity levels of the image. Since there are a large number of dots in the image, the peak intensity value at the histogram tail should represent a large number of the pixels contained in the dots. This global threshold was applied to the original greyscale image.

Figure 5.7, Image After Global Thresholding, Method 1



From figure 5.7, it is obvious that this method of global thresholding is inadequate. The global threshold level is too low, as it allows the pixels from the top right hand corner to become white. The top right hand corner is affected by the arc light more than other background areas, which causes that area to have higher intensity values than other areas of the background.

Figure 5.8, Histogram Intensity Range for Method 2 of Global Thresholding



The second global thresholding method uses multiple local threshold levels to calculate a final global threshold. Figure 5.8 shows a histogram where a range of intensity values (shown by the red lines) in the input image is used to calculate a threshold value. In this second method of global thresholding, the maximum intensity value of the histogram is found, as well as the intensity value corresponding to the majority of the pixels. These values are averaged and a small offset is added to create a threshold value for the entire image.

Figure 5.9, Global Threshold Value: Method 2

$$T_{global_2} = \frac{I_{max} + I_{majority}}{2} + I_{offset}$$

Through a few experiments, an offset value of 15 grey level units was found to produce optimal results.

Figure 5.10, Image After Global Thresholding, Method 2

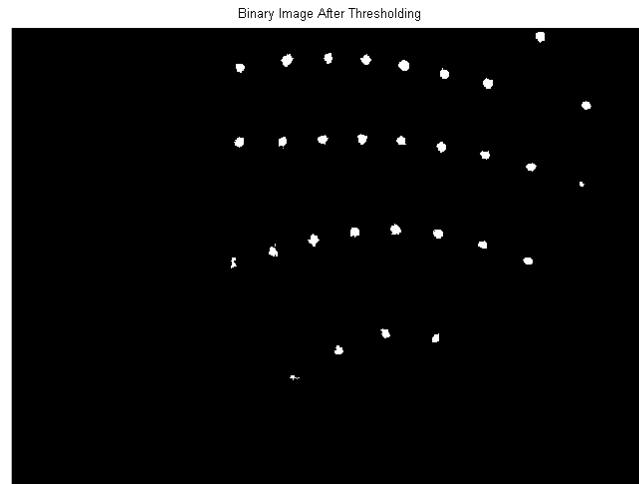


Figure 5.10 shows an image after thresholding with this second method. This is a much improved image than the first global thresholding method, and each dot's shape is clearly visible. When compared to the original image in figure 5.3, it is apparent that the bottom right dot is missing. This indicates that this method of global thresholding does not have high enough contrast since the bottom right dot is visible in the original image. Global thresholding is inadequate for these types of images, so a different thresholding method must be applied.

Adaptive Thresholding

Adaptive thresholding uses multiple local threshold levels to extract the desired subject from the background. The threshold levels change dynamically as the input image is parsed [8]. The same basic operation as global thresholding ultimately applies:

an input image pixel is compared against a threshold, and the corresponding output image pixel is either a '1' or '0' depending on the input pixel's intensity.

The adaptive thresholding method used is block thresholding. The image is divided up into 768 blocks of 20x20 pixels, and the average intensity value of the pixels in each block is calculated. Each pixel in the block is then parsed and compared against the average intensity value of the block, and thresholding is applied. The size of the blocks chosen was experimentally found to give the best results.

Figure 5.11, Block Thresholding Equations

$$B_i[x, y]_{output} = \begin{cases} 1 \rightarrow B_i[x, y]_{input} \geq T_i \\ 0 \rightarrow B_i[x, y]_{input} < T_i \end{cases} \quad i = 1:n$$

$$T_i = Avg_Intensity(B_i) + T_{offset}$$

In figure 5.11, $B_i[x, y]$ represents the pixel location in the i 'th block, while B_i represents the i 'th block of the image. Again, experiments showed that this dynamic thresholding method would perform better with a small offset, so T_{offset} was chosen to be 18 units of grey level intensity.

Figure 5.12, Binary Image After Block Thresholding

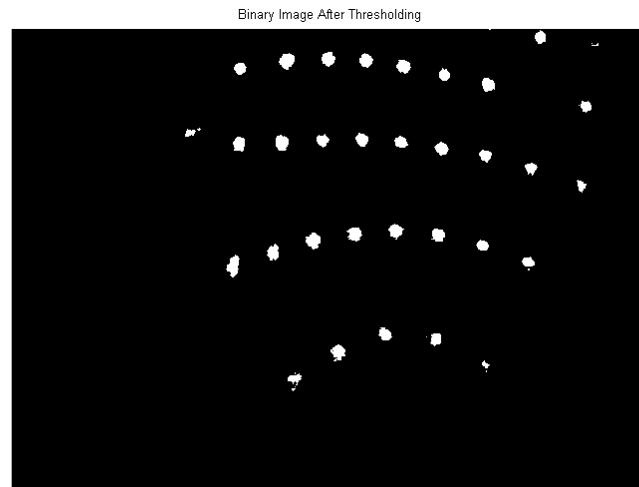


Figure 5.12 shows the binary image from the block thresholding method. The shapes of the dots in this method are not as smooth as global thresholding, but this method does extract every dot. Edges of the dots are rough and there is background noise visible. To improve this image, the next step of the image processing algorithm must be completed.

Median Filtering

In figure 5.12, there is some background noise visible as small white speckles near the edges of the dots and from any dots that did not provide enough contrast to be extracted. This type of noise in an image is defined as “salt and pepper” noise [9]. The name comes from the fact that the noise will appear as small white dots (salt) in a black background or small black dots (pepper) in a white background. Pepper noise is also present and contributes to the dots’ irregular shapes. Salt and pepper noise is also known as impulsive noise since the pixel will be either white or black (1 or 0).

Figure 5.13, Salt and Pepper Noise Model (Impulsive Noise)

$$X_{noisy}[n] = \begin{cases} X[n] & (1 - P)\% \text{ of time}, \text{ value of noise : } 0 \\ +1 & (P/2)\% \text{ of time}, \text{ value of noise : } +1 \\ 0 & (P/2)\% \text{ of time}, \text{ value of noise : } -1 \end{cases}$$

Figure 5.13 states that the probability of a pixel being composed of noise is P . Thus, the pixel will not be affected by noise $(1 - P)\%$ of the time, while being composed of noise $P\%$ of the time. From figure 5.13, there is an equal probability that the noise will cause the pixel's intensity to reach its maximum value of 1, or a minimum value of 0.

Figure 5.14, Probability Graph for Salt and Pepper Noise

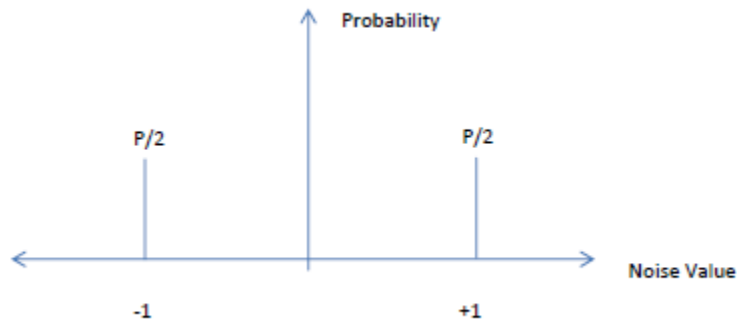


Figure 5.14 shows a graphical representation of salt and pepper noise. It shows that there is an equal probability of injecting a value of +1 or -1 for salt and pepper noise. As stated, if 1 is the noise value, the pixel will become a 1, and if -1 is the noise value, the pixel value will be clipped to a 0. If no noise is present, the pixel will not be affected and the value of the noise is 0.

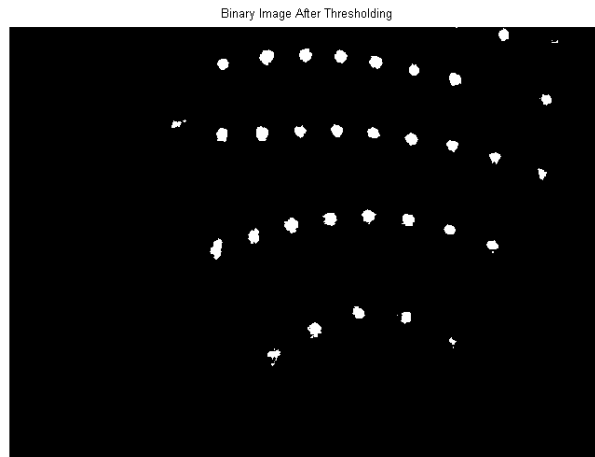
To eliminate salt and pepper noise in an image, a median filter is the classic choice. A median filter is a neighborhood process that replaces a pixel's value with the median of its neighboring pixels. The median is calculated by sorting all of the pixel values in the neighborhood in increasing order and then replacing the center pixel with the middle pixel value [8]. If the number of pixel values is even, the average of the two middle pixels is used. For the reflected dots image, a 3x3 median filter is chosen as the filter size.

Figure 5.15, 3x3 Median Filter Window

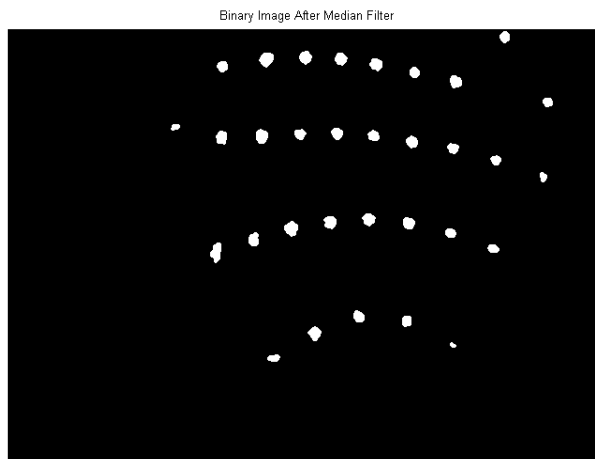
0	0	0
0	1	1
0	0	0

Figure 5.15 shows a 3x3 window of an image. In this case, the middle pixel is unrepresentative of its neighboring pixels since the majority are 0's. When the median filter operation is performed, the center pixel in figure 5.15 will be replaced by a 0, thus eliminating the sporadic 1 (white pixel) in this block of the image. The median filter is applied to the whole image in a sliding window fashion to eliminate most of the intermittent white pixels.

Figure 5.16, Binary Image (a) Before Median Filter, (b) After Median Filter



(a)



(b)

Looking at figure 5.16 (b), the background noise that contributed to intermittent white speckling was removed. Also, the pepper noise was reduced which enhances the circular shapes of the dots. Even after median filtering, some of the dots appear as polygons instead of circles. Thus, the next step in the dot extraction algorithm is morphological operations to exaggerate the circular shape.

Morphological Operation

The morphological operation used on the image after filtering is dilation. This will produce an image of circular dots with smooth edges. Dilation requires two data elements as inputs [9]:

- 1) Image that is to be dilated
- 2) Dilation Kernel

The image to be dilated is the output from the filtering step, while the dilation kernel is a 3x3 element that contains all 1's. The kernel is superimposed over the input image so that the center of the kernel coincides with each input pixel location. If at least one pixel in the kernel coincides with an input pixel location, then the input pixel is set to a 1 [9].

Figure 5.17, Morphological Operation: Dilation [10]

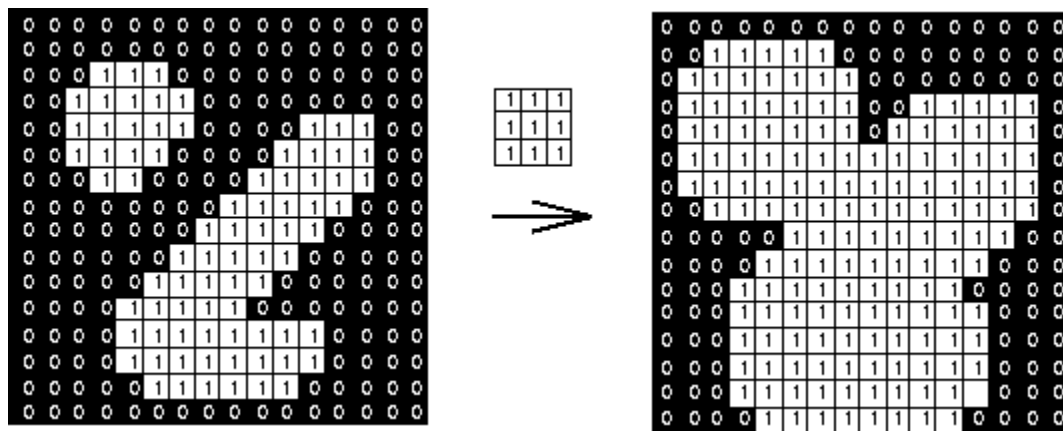


Figure 5.17 illustrates this concept for a 3x3 square kernel. Figure 5.17 shows how the dilation kernel slides across the entire image pixel by pixel, and will replace 0's with 1's based on the condition already described.

Figure 5.18, (a) Image Before Dilation, (b) Image After Dilation

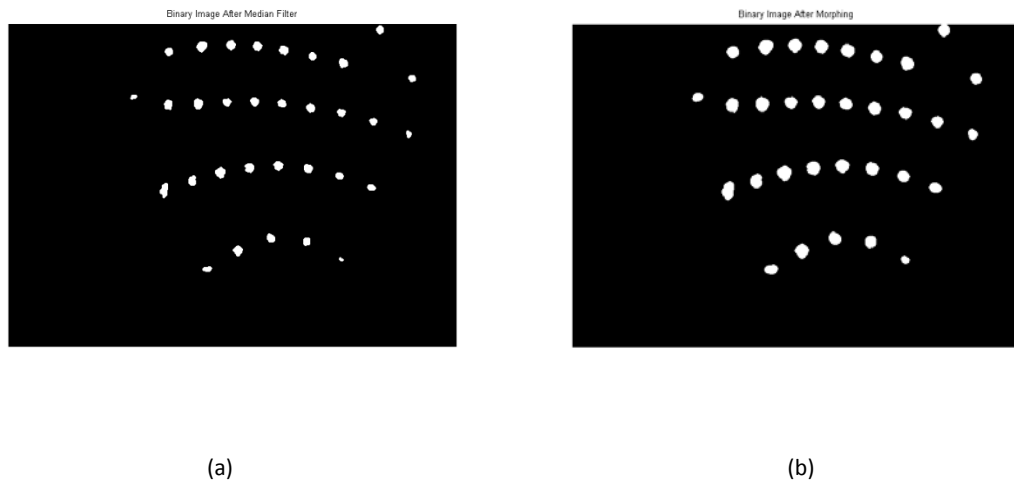


Figure 5.18 shows the image before and after dilation. The dots clearly have more of a circular shape with smoother edges. The image after dilation will be used for all position information; dilating the circles will make it easier to calculate the centroid of each dot.

Centroid Calculation

The centroid is calculated by finding the intersection of the lines that represent the height and width of the reflected dot.

Figure 5.19, Centroid Calculation

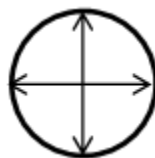


Figure 5.20, Original Greyscale Image with Center of Reflected Dots Shown, 80A

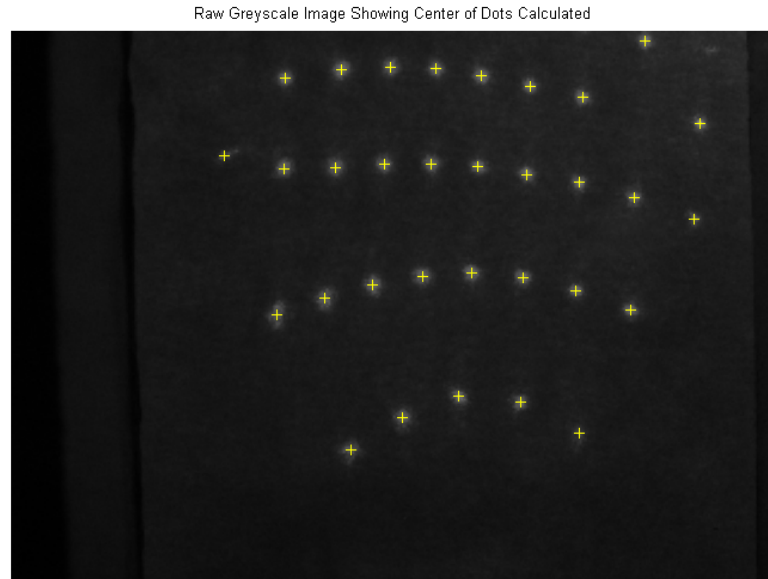


Figure 5.20 shows the original greyscale image with crosshairs at the center of each reflected dot.

Figure 5.21, Original Greyscale Image with Center of Reflected Dots Shown, 125A

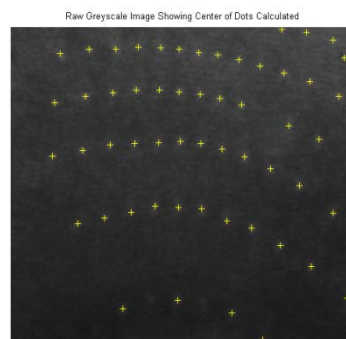
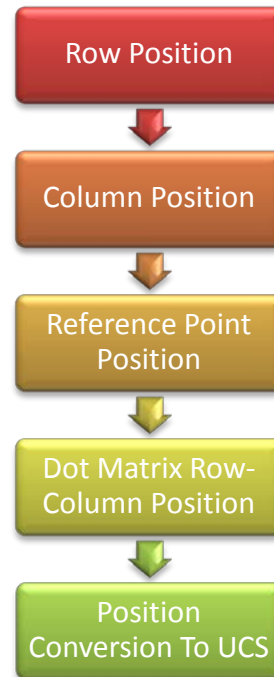


Figure 5.21 shows the centroid calculation with the welding current at 125 amps. The centroids are still able to be extracted even though the image has low contrast due to the bright background.

Position Information Extraction

The flowchart for the position information extraction is shown in figure 5.22.

Figure 5.22, Position Information Extraction Flowchart



Row Position

The row position is defined by the flowchart in figure 5.23. The goal is to find dots that are in the same row: the sequence of the rows will be addressed after all dots have an associated row. The first step is to create a structure of all the dots' image coordinates. The leftmost dot in the X direction will be used as the starting dot in the first row. This dot is then removed from the structure, since its row position has been identified. To find dots that are contained in the same row as the starting dot, Euclidian distance and angle information is used as criteria. If the nearest dot from the previous identified dot is less than 40 degrees and greater than -60 degrees, the dot is identified as the next dot in the row. The angle requirements are with respect to the positive X

axis. When a dot's row position is identified, it is then deleted from the structure. If the nearest dot does not satisfy the angle requirements, the end of the row has been found. The process is then repeated by finding the leftmost dot of the remaining dots in the structure. When the structure is empty, all dots' row positions have been identified. Since the beginning dots of each row are determined by which is furthest to the left, the Y positions of each row are not in order. It is then easy to parse the coordinates of each row position so that row 1 is at the bottom of the image, and row n (where n is number of rows) is at the top of the image. Any row that contains only 1 dot will be removed.

Figure 5.23, Row Position Flowchart

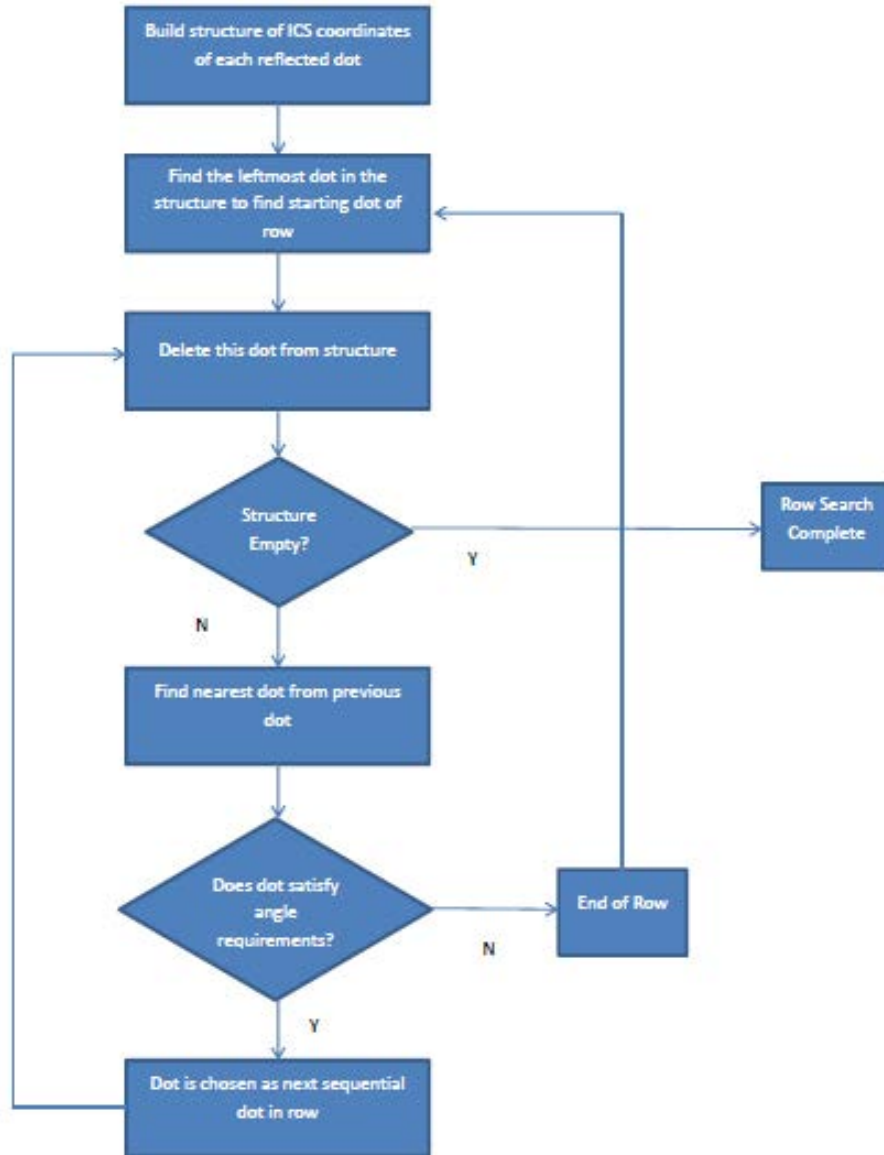


Figure 5.24, (a) Row Parsing Order and Angle Requirements, (b) Rearranged Rows in Increasing Order

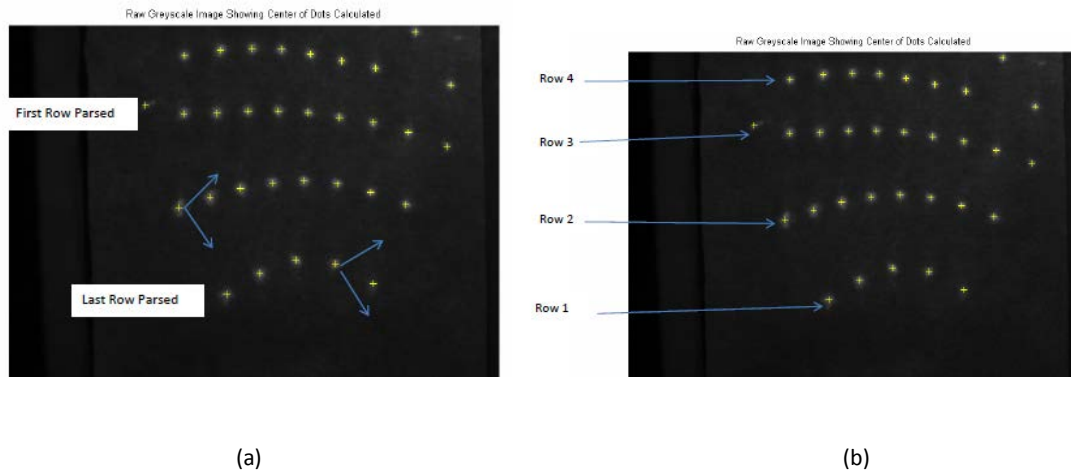


Figure 5.24 (a) shows the order the rows are parsed and the angle requirements that the next dot must fulfill. Figure 5.24 (b) shows how the rows are sequenced in increasing order.

Column Position

Once every dot has been associated with a particular row, the dots must be associated with a particular column. The column position extraction is simpler than the row position analysis. All that is needed is to find one dot in each row that is in the same column, and the column location of the remaining dots can be found. To find the first column, distance is used to find the dots that are very close together in the horizontal direction. The row that contains the most dots is used as a starting point, and the remaining dots in the image are searched to find the nearest neighbors in the horizontal direction. Once a nearest neighbor is found in every row, this column becomes the reference column. Figure 5.25 shows the flowchart to identify the reference column.

Figure 5.25, Reference Column Identification

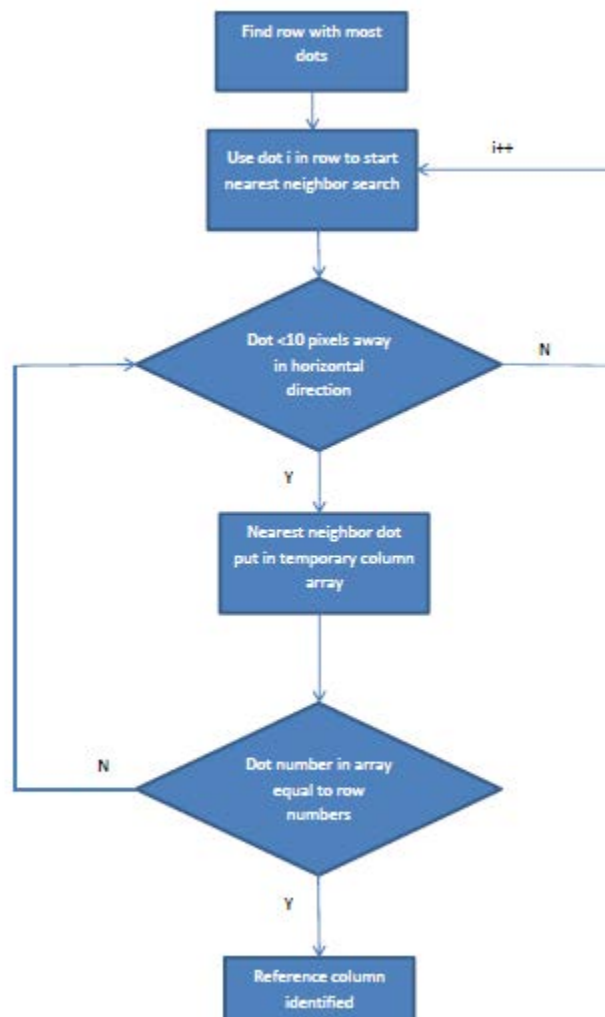


Figure 5.26, Reference Column



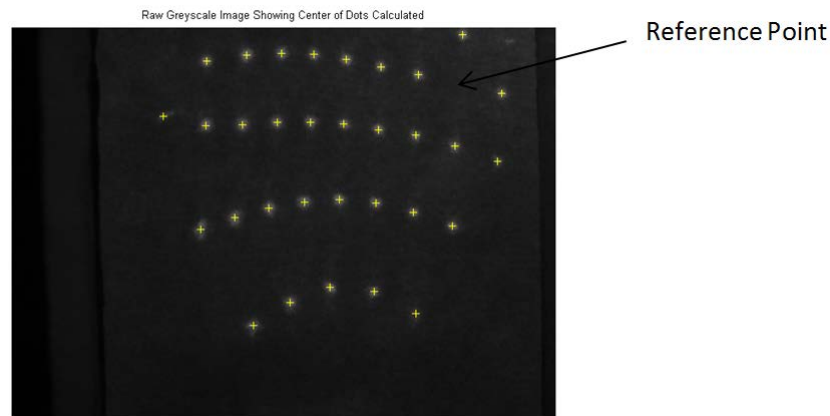
Figure 5.26 shows the reference column in the image, which is identified by the red line.

Once a reference column location in each row is found, the relative column location for the remaining dots in each row can be determined. To find each dot's row-column position in the dot matrix, the reference point must be found.

Reference Point Position

The reference point in the image will indicate a position of row 10-column 10 in the dot matrix pattern. Locating the position of the reference point requires finding two dots in a row that exhibit a larger than average gap between the two dots.

Figure 5.27, Reference Point Location

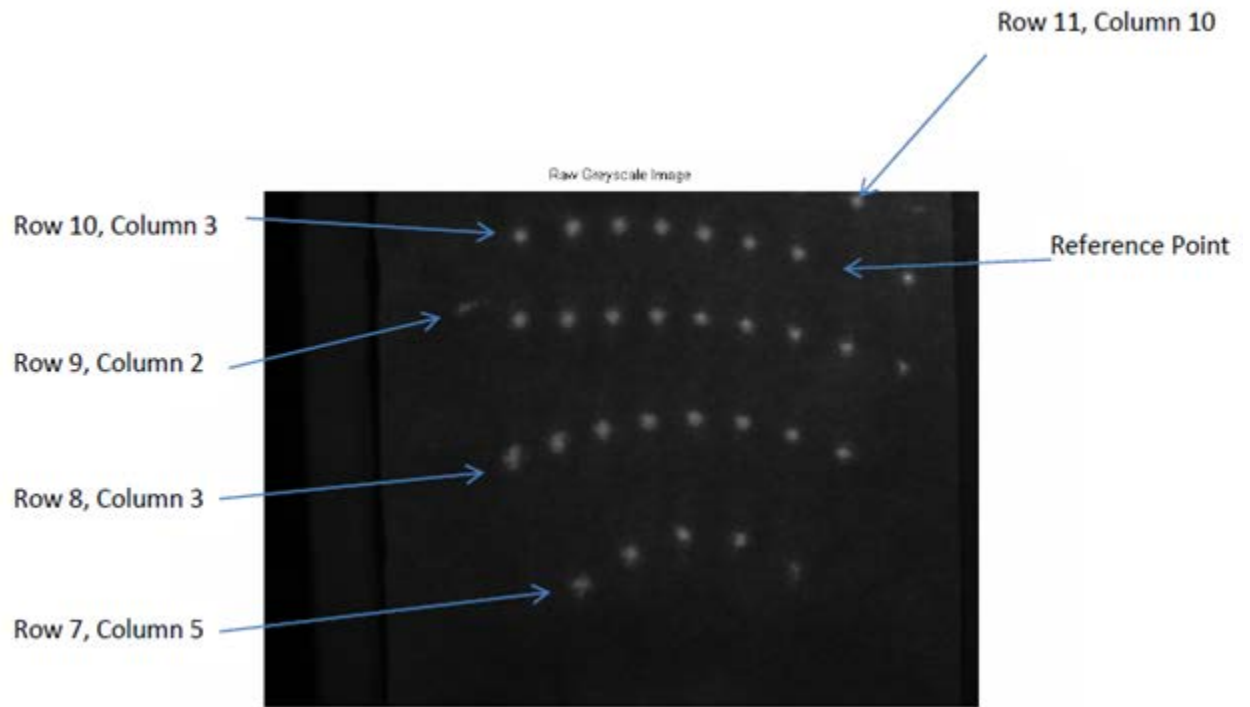


During row position analysis, the average horizontal distance between all dots is calculated. Thus, all that is necessary is to find the two dots where the horizontal distance is much greater than average. To calculate the image coordinate system position of the reference point, the positions of the two dots that surround the reference point are averaged. The position of the reference point can now be used to calculate the dot matrix positions of every dot in the image.

Dot Matrix Row-Column Position/UCS Conversion

Every dot can now be assigned a dot matrix row-column number. Since we are assuming a convex weld pool surface, the position relationship between the laser shining onto the weld pool and the reflected image will be sequential. The reference point is defined at row10-column10, so each dot in that row is part of row 10. The dot matrix row numbers of the remaining dots can now be easily found. The dots on either side of the reference point will have a column number of 9 and 11. The reference column can now be assigned a dot matrix column number, and the dot matrix column number of the remaining dots can be found.

Figure 5.28, Dot Matrix Position of Reflected Dots



Each dot's centroid in the reflected image has an X, Y position in image plane coordinates, and an associated dot matrix row-column number. The image plane coordinates can be converted to the universal coordinate system using the equation in figure 4.3 for input into the weld pool reconstruction algorithm.

6. Real Time Reconstruction of 3D Weld Pool Surface

The results from the previous image processing algorithms provide the necessary information to calculate the weld pool surface. The 5 inputs to the weld pool reconstruction algorithm are:

- 1) Centroid universal coordinates of each reflected dot
- 2) Dot matrix row-column positions of each dot
- 3) Universal coordinates of reference point
- 4) Universal coordinates of laser
- 5) Universal coordinates of imaging plane center

A weld pool surface reconstruction can be computed for each image that is captured by the camera. Real time processing can be achieved by continually processing images from the camera, and applying the weld pool reconstruction algorithm on these images. This processing can also be applied to videos of the dots reflecting from the weld pool. Running the “real time processing” algorithm on videos was used to verify the processing algorithms and provides a demonstration for the methods developed. The difference between processing data from the camera in real time and from videos is the data path to the MATLAB image processing.

Figure 6.1, Weld Pool Reconstruction Data Path

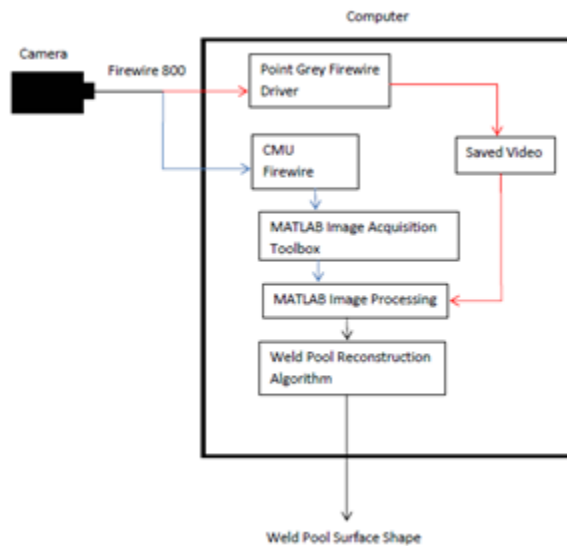


Figure 6.1 shows the data path from the camera to the reconstructed weld pool surface shape. Using the Point Grey driver that was included with the camera, data can be saved to the hard drive in AVI video format and each frame will be captured by the MATLAB image processing module. The real time processing path uses the MATLAB image acquisition toolbox to acquire frames from the camera via an open source CMU firewire driver. The output from the image acquisition toolbox can then be input to the MATLAB image processing module. Each path converges at the MATLAB image processing module before the 3D weld pool reconstruction algorithm. To understand how the weld pool shape is obtained, a summary of the weld pool reconstruction algorithm is presented.

Brief Summary of Weld Pool Reconstruction Algorithm

A complete detailed explanation of the weld pool reconstruction algorithm can be referenced in HongSheng Song's dissertation "Machine Vision Recognition of Three

Dimensional Specular Surface for Gas Tungsten Arc Weld Pool [1].” The base MATLAB code for the weld pool reconstruction algorithm was obtained from HongSheng Song, and modified for the compact vision system. A summary of the method used for this research will be presented. Several methods have been developed for the surface reconstruction, but the simplest method was chosen for real time reconstruction to increase speed.

The simulations in chapter 4 determined the reflected image from a known weld pool surface. Weld pool reconstruction is an inverse problem: calculate the weld pool surface from the reflected image. The goal is to find a corresponding 3D point in the weld pool for each 2D point in the imaging plane.

The weld pool surface is assumed to be flat in the first iteration of the reconstruction algorithm. Each projected point can then be calculated on this “flat weld pool” surface similar to the simulations in chapter 4. As discussed in chapter 4, the normal vector to the projected point on the weld pool surface will bisect the incident ray and reflected ray. Since the initial surface is assumed flat, the normal vector from the surface point will obviously not fulfill this condition. The ray that bisects the projected point on the initial flat surface and the reflected point will be used as an initial calculation of the weld pool point’s normal vector. From this initial normal vector, a tangent plane can be found to start the reconstruction of weld pool points for each reflected dot. Once an initial pass of the weld pool surface is complete, the normal vector from each point on the surface (which is now not flat) will be compared to the

ray that bisects the incident and reflected rays. If this comparison shows that the normal surface vector and bisecting ray are close, then an accurate weld pool surface has been reconstructed.

By using the law of reflection, the normal of every reflection point $p_{i,j}$ on the weld pool surface can be computed from the corresponding incident and reflected rays. This normal is defined as the ray that bisects the incident and reflected rays. The tangent plane at every reflection point can then be computed, which is referred to as its 3D slope. The intersection of this tangent plane with the row plane provides a 2D slope, or row slope [1]. Conversely, the intersection of the tangent plane with the column plane provides a column slope [1].

Figure 6.2, 2D Slope Diagram [1]

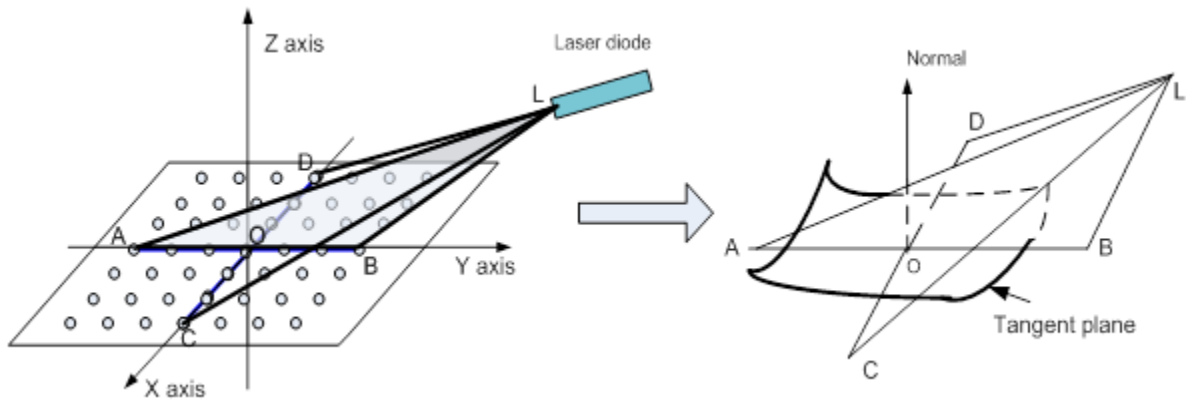


Figure 6.2 shows the different planes used to calculate the row and column slopes of each reflected dot on the weld pool surface. The tangent plane is clearly visible. Plane LDC is the row plane, while LAB is the column plane. The intersection of the tangent

plane and plane LDC forms the horizontal 2D slope (row slope), while the intersection of the tangent plane and plane LAB forms the vertical 2D slope (column slope).

Figure 6.3, Row Slope Calculation Diagram

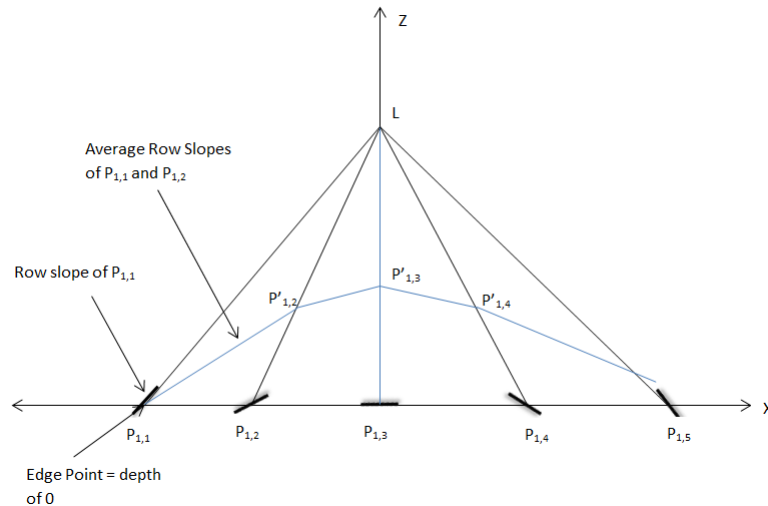


Figure 6.3 shows a diagram of each projected point in a row, labeled as $P_{1,j}$. The row slopes of each point are visible, and the path of the incident ray from the laser (labeled as L) is also visible. Starting with the corner edge point ($P_{1,1}$) which has an assumed depth of 0, this point's row slope and the consecutive point's row slope are averaged together. The intersection of the average row slope and the incident ray from the laser create a new weld pool point, labeled as $P'_{1,2}$ in figure 6.3. This process is continued for the rest of the dots in the row, ending on the other edge point in the row. The middle point in the first row is used to calculate a middle reference column, which assists in calculating the points of the dots in the remaining rows. To calculate a point in the transverse direction as the row, column slopes must be used.

Figure 6.4, Column Slope Calculation Diagram

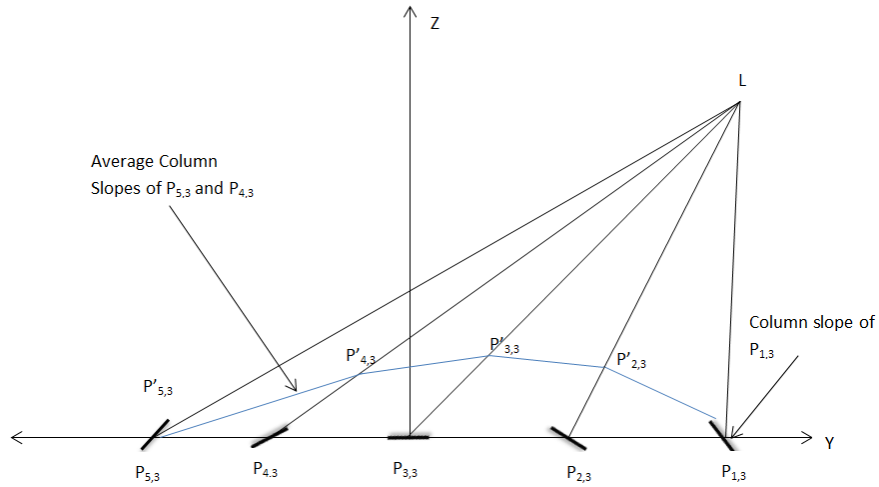


Figure 6.4 shows a diagram of the column slope calculation, which is similar to the row slope calculation diagram. In figure 6.4, point $P_{1,3}$ is the middle point in the first row, and has known weld pool point coordinates from the previous row slope operations. From this known point, the middle column weld pool points are calculated along the -Y axis to create a known weld pool point in each row. Again, the average column slope between $P_{1,3}$ and $P_{2,3}$ is found, and the intersection of this slope with the laser ray will create a new weld pool point, $P'_{2,3}$. The column slope operations are continued for the remaining dots in the middle column.

One Point Algorithm

The weld pool reconstruction algorithm used is called OPA, or One Point Algorithm [1]. The depth of one edge point is assumed to have a depth of zero because it is at the boundary of the weld pool. This edge point on the weld pool is the same as its projected point on a flat surface. Having a starting point to work with, the row slopes of the rest of the dots in the first row can be calculated.

Figure 6.5, OPA Parse Directions

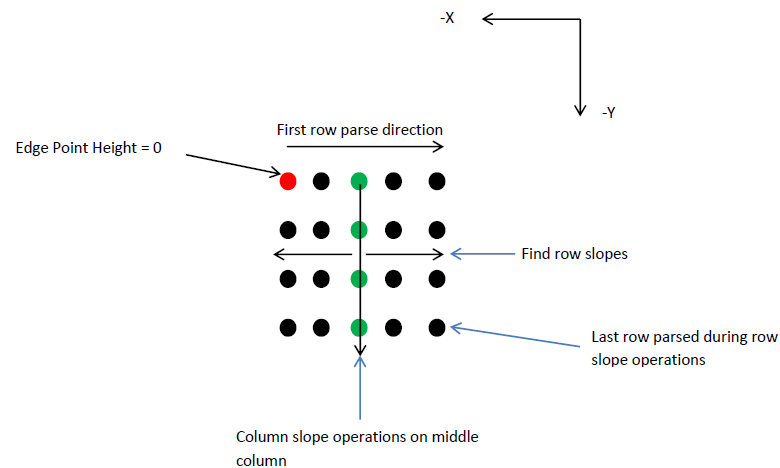
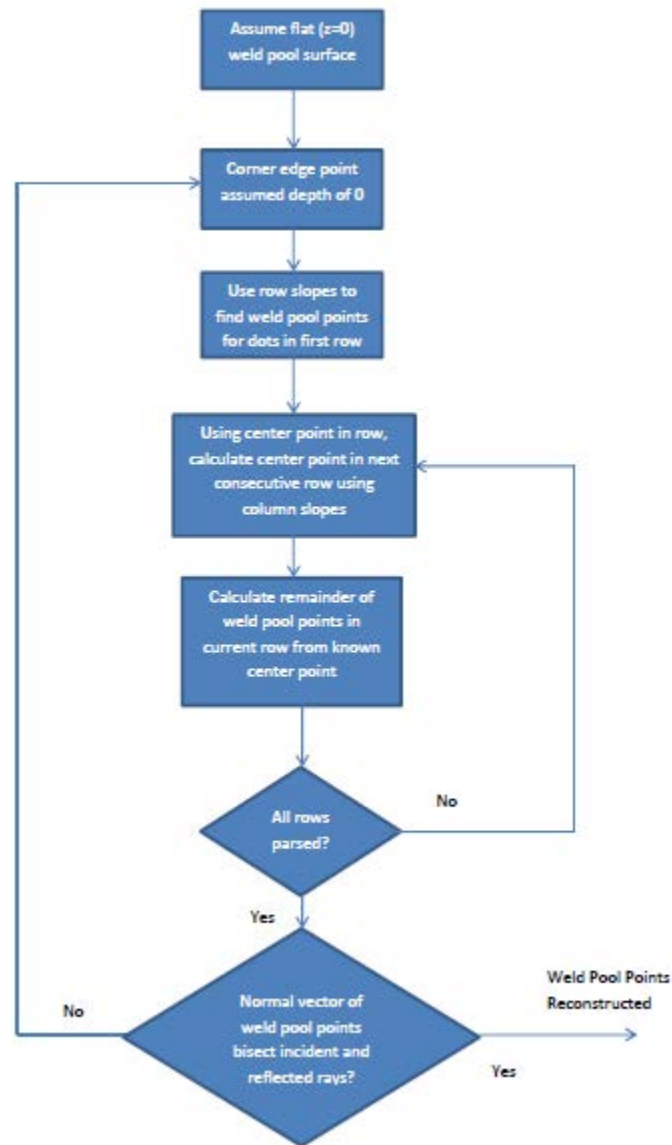


Figure 6.5 shows how the dot matrix is parsed to calculate the weld pool surface. Using the corner edge point as a known point (red dot in figure 6.5), the weld pool surface points in the first row can be calculated using row slopes. Using the center dot in the first row, the middle column points (green column in figure 6.5) can be calculated by using column slopes. This provides a known point in the middle of each row. Row slopes can be calculated from the center of the rows towards the edges to find the points of the remaining dots in each row.

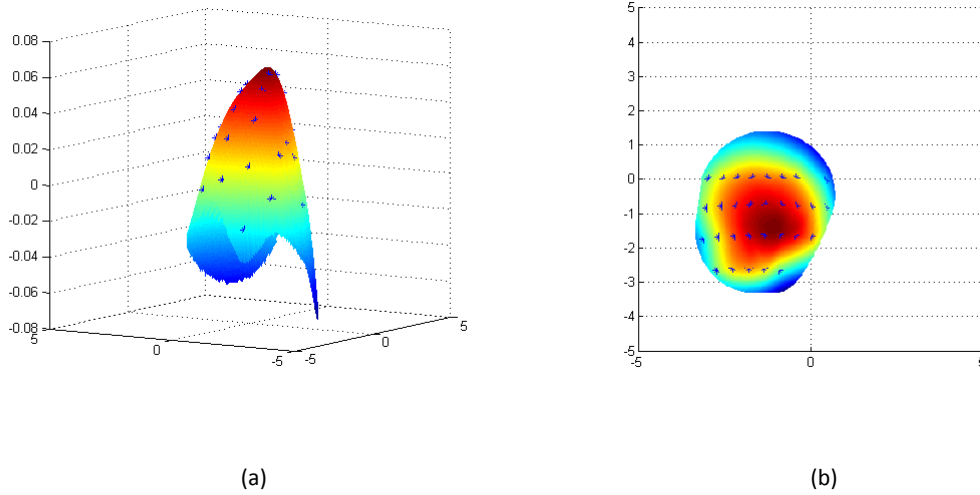
The process starts over with the newly calculated weld pool points as the weld pool surface, and is repeated several times until the normal vector projected from each weld pool point nearly bisects the incident and reflected rays. The more loops that are run on the OPA algorithm, the more accurate the weld pool surface shape. Figure 6.6 shows the flowchart of the OPA algorithm that has been described.

Figure 6.6, Flowchart of One Point Algorithm



The output of the weld pool reconstruction will be a weld pool surface interpolated from the universal coordinates of the weld pool points, as shown in figure 6.7. Figure 6.7 (a) shows the weld pool from the side; while figure 6.7 (b) shows the weld pool from the top (Z-axis is amplified to enhance shape of weld pool). The projected dot matrix points are clearly visible in each figure.

Figure 6.7, Interpolated Weld Pool Surface (a) Side View, (b) Top View



A B-spline interpolation method in MATLAB was used to create the final weld pool surface from the discrete weld pool points [11].

Figure 6.8, 1-D B-Spline Cubic Interpolation Formula [9]

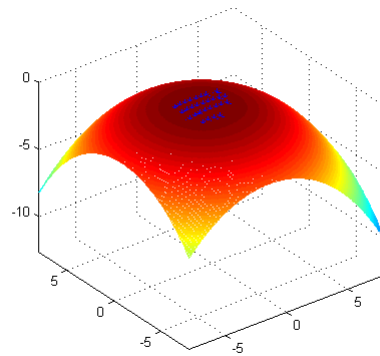
$$f(x) = \begin{cases} \frac{1}{2}|x|^3 - |x|^2 + \frac{2}{3} & 0 \leq |x| < 1 \\ -\frac{1}{6}|x|^3 + |x|^2 - 2|x| + \frac{4}{3} & 1 \leq |x| < 2 \\ 0 & \text{else} \end{cases}$$

Figure 6.8 shows a one dimensional B-spline cubic interpolation formula. The interpolated points are determined by how far away they are from the known points. This equation shows that the output can be influenced by a maximum of 4 points.

If the imaging plane is unable to capture all the reflected dots, the weld pool surface can be extrapolated from the known weld pool surface. To simulate the

extrapolation, a size of 8 mm was chosen for the weld pool radius boundary. Figure 6.9 shows the extrapolated weld pool, with the dot matrix pattern clearly visible at the apex of the weld pool surface. A built in MATLAB B-spline quadratic extrapolation in each direction was used [11].

Figure 6.9, Extrapolated Weld Pool Surface

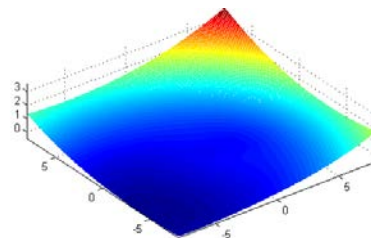


As a comparison, an image captured during the beginning of the welding process was input to the image processing/weld pool reconstruction algorithms. This image in figure 6.10 (a) does not exhibit much curvature, so the extrapolated weld pool surface in figure 6.10 (b) is relatively flat.

Figure 6.10, (a) Centroids of Image at Start of Welding Process, (b) Flat Extrapolated Weld Pool



(a)



(b)

Weld Pool Reconstruction Error

The weld pool points that were calculated in the reconstruction algorithm were run through a simulation to calculate the difference between the actual and computed reflection points. Figure 6.11 shows the actual reflection points from the imaging plane in blue, and the points reflected from the simulated reconstructed weld pool surface in red.

Figure 6.11, Error Between Actual and Computed Reflection Points

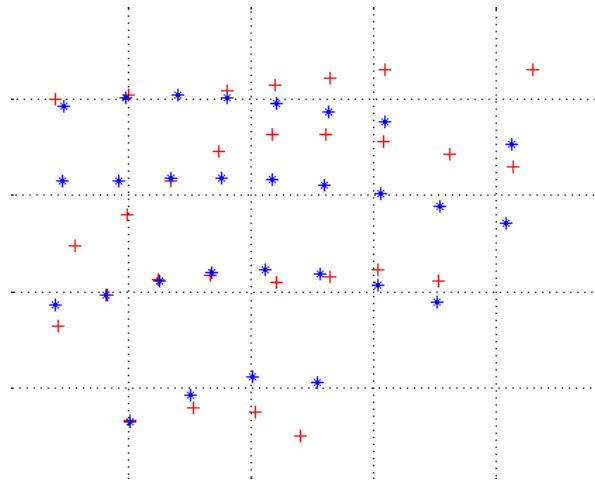


Figure 6.11 indicates that the reconstructed weld pool is close to the actual weld pool surface, but there is still some error. There are many sources of error in the compact vision system.

The software contributes error during the image processing and weld pool reconstruction. The extraction of each reflected dot's centroid contains error. During the dilation step, the dots are enlarged to ease centroid calculation, but this might shift the exact center of the reflected dot. In the weld pool reconstruction algorithm, the reconstructed weld pool surface will never be exact. This is due to the curved surface of

the weld pool being approximated by small linear pieces. The OPA algorithm was used for its increased performance, but other methods could be used to create a slightly more accurate weld pool surface.

The hardware also contains many sources of error. The small imaging plane only allows a certain number of reflected dot matrix points to be captured. The more dots that are reflected onto the imaging plane, the more information received about the weld pool surface. Thus, if the weld pool becomes large enough, the error from the small imaging plane will increase. Measurement error in the compact vision system also contributes to the hardware error. This error includes the angle of the laser and various universal coordinates of the components. The torch also contributes some error, as it is not perfectly at the apex of the pipe, and the tip might not be perfectly aligned with the $-Z$ axis. Since the compact vision system is attached to the torch, vibrations during welding also induce error.

Real Time Reconstruction Results

Weld pool reconstruction using the MATLAB image acquisition toolbox enabled the monitoring of the weld pool surface shape in real time. The definition of “real time” in this research is the ability to monitor the quality of the welding process (via weld pool surface reconstruction) without sacrificing welding speed. The MATLAB image acquisition toolbox is able to access the Point Grey camera via the CMU driver (an open source firewire driver developed at Carnegie Mellon University). The entire camera’s settings (resolution, color/greyscale, white balance, gain, shutter, etc.) can be initialized

with a few lines of MATLAB code. Frames directly from the camera are sent to the image processing and weld pool reconstruction algorithms during welding.

Greyscale images of the reflected dots from 10 consecutive frames are shown in figure 6.12.

Figure 6.12, Consecutive Greyscale Images During Real Time Processing

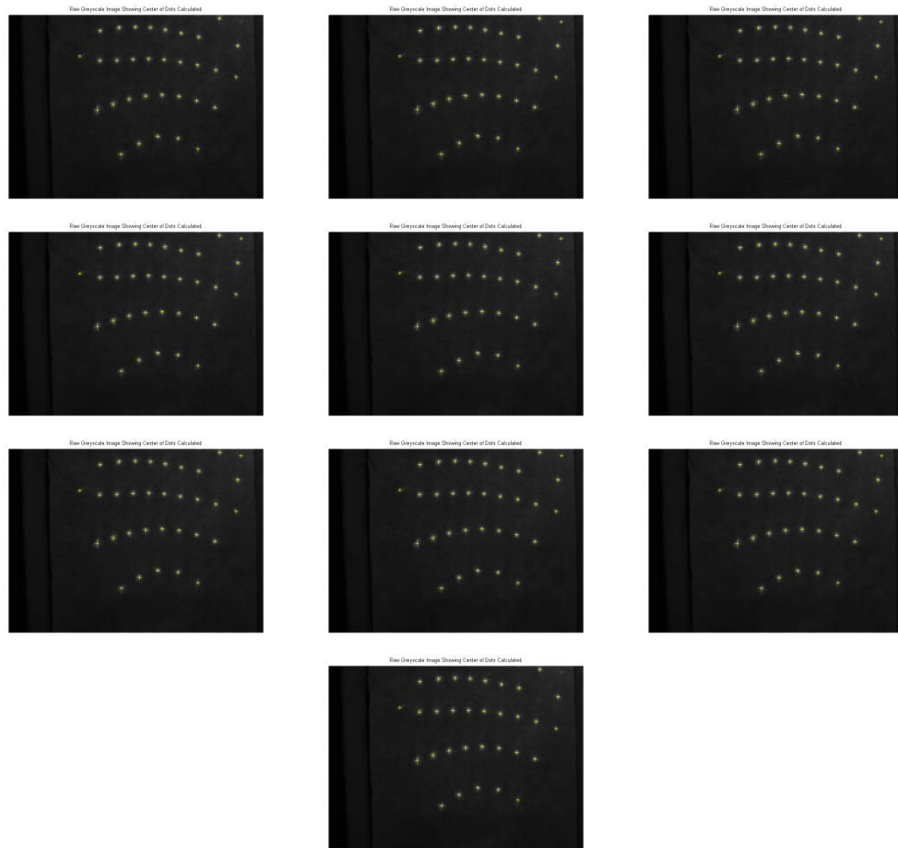
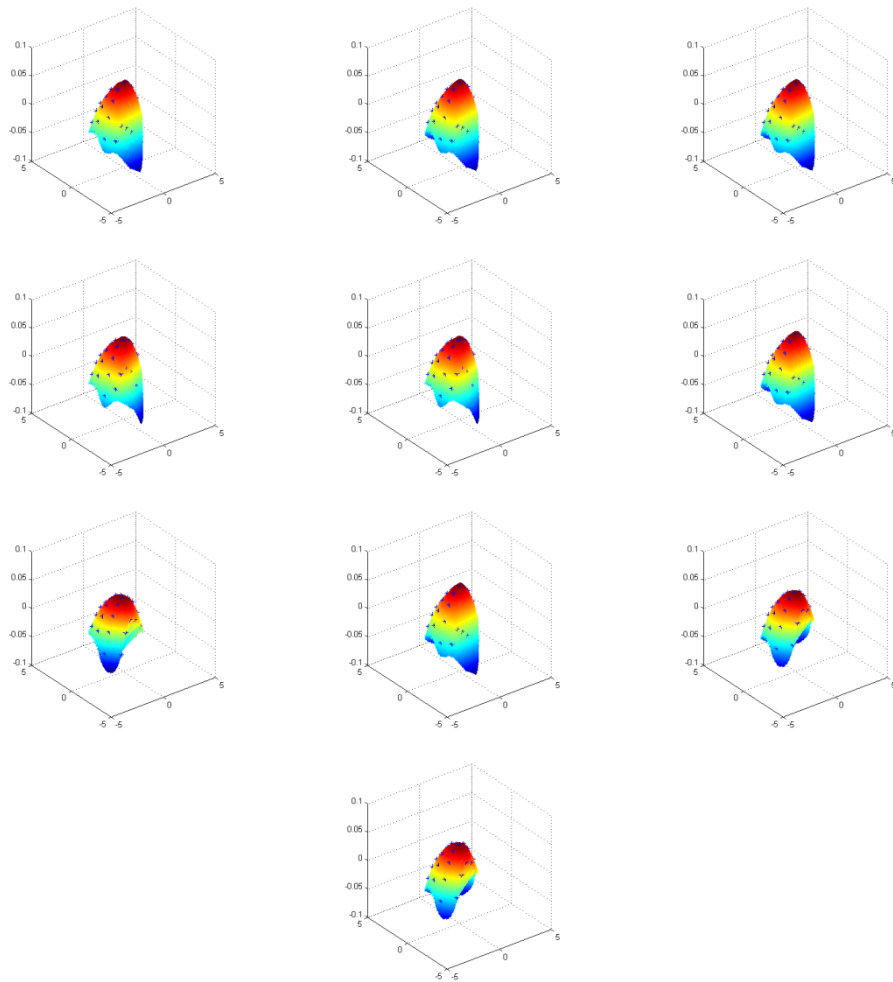


Figure 6.12 includes crosshairs to indicate the centroids. The universal coordinates of the centroids of each reflected dot are calculated in real time and input to the reconstruction algorithm for monitoring the 3D weld pool surface. The corresponding weld pool surfaces to the greyscale images in the previous figure are shown in figure 6.13.

Figure 6.13, Real Time Reconstructed Weld Pool Surfaces



The Z axis in figure 6.13 is amplified to exaggerate the shape of the weld pool. Weld pool oscillation is visible as the images progress.

Real Time Performance

The surfaces in figure 6.13 represent just 10 frames of video (where frames are acquired at 60 frames per second). The MATLAB profiling tool was used to measure the performance of the software for 100 images. The image processing portion of the MATLAB software took 2 seconds to find the centroids of 100 images. Finding the 3D universal coordinates of the weld pool surface took 5 seconds, and interpolating the

surface took 35 seconds, for a total time of around 42 seconds to interpolate the weld pool points for 100 images. Capturing the images from the firewire camera consumed about 2 seconds of processing time, for a total time of 44 seconds to interpolate a reconstructed weld pool of 100 images captured in real time. The frames from the camera can be acquired sequentially and stored, or each frame can be acquired after the reconstruction is finished on the previous frame. For the performance calculations, the weld pool reconstruction was performed before the next frame was acquired from the camera. Since the software cannot keep up with the high frame rate of the camera, acquiring images in intervals is the only way to achieve real time processing. The MATLAB code was run on a low end processor running at 2.4 GHz, with 2GB of RAM and integrated graphics.

MATLAB can reconstruct the 3D weld pool surface at 2.4 frames per second and the image processing portion can find the centroids of the dots at around 50 frames per second. The weld hat of the orbital pipe welding machine contains motors to move the torch to the next welding position. Moving the torch will ultimately be the limiting factor in the system since the movement of the electric motors will be an order of magnitude slower than the software. The welding torch operating at 80 amps will stay in the same place for multiple seconds until a quality full penetration weld is achieved. Previous research has established “real time” as 4 frames per second to determine the area and boundaries of a weld pool [12]. The 4 frames per second allowed the weld pool area to be detected in 0.5 millimeter resolution. Thus, 2.4 frames per second is a little low for real time processing throughput. Nevertheless, it is much faster than a

human can monitor a weld pool surface. Since the goal of this research is to determine if weld pool monitoring is achievable in the compact vision system, there are some easy steps to increase the processing throughput.

The number of frames per second processed in this research is a direct result of the computer used, since the software is written in MATLAB. Since a low end laptop was used, higher throughput can be achieved with increased computing capacity. A computer with a more powerful processor, more memory, and discrete graphics processor will be able to achieve many times the performance compared to the computer used in this research.

7. Conclusion

This research demonstrated the feasibility of the compact vision system for the monitoring of a 3D weld pool surface, which has been a major hurdle in welding research. Creating a system that can be mounted directly to the welding torch to monitor the 3D weld pool surface in real time is a huge achievement. Future work on the compact vision system can enable it to be used in a commercial system. Even though pipe welding was used in this research due to the ease of automation, this compact system could be applied to other methods of automatic welding.

Quality images of the dot matrix reflecting from a convex weld pool surface were obtained and it was proved that these images from the compact vision system could be used to reconstruct and monitor the weld pool surface. Even though real time processing throughput was a little less than required, the purpose of this research is to demonstrate that real time monitoring of a weld pool surface is feasible in this compact system. Increasing the processing power of the software will easily achieve the required throughput for real time monitoring.

The real time centroid monitoring of the reflected images can be applied to other areas of computer vision. Being able to track the positions of fiducial points can be used in medical imaging, astronomy, sports, etc. Any application where points are extracted from a background and tracked could be potential targets of the real time centroid monitoring.

This research has produced good results, and proves a vision system can be mounted to a weld torch to achieve real time monitoring of the weld pool surface. This

has been achieved even though there are many restrictions in the compact vision system. The main restriction is the size of the imaging plane: to have a compact fixture, the imaging plane must be extremely small. The more dots that are able to be reflected onto the imaging plane, the more accurate the weld pool surface reconstruction. Filling up the entire imaging plane in the compact vision system with dots has produced satisfactory results in terms of producing a weld pool shape. In some images, the welding torch tip blocks some of the dots at the top of the image. This has been documented in previous research, and is unavoidable [1, 13]. The welding tip cannot be more than a few millimeters from the work piece and will inevitably block some of the rays from the laser. Overall, this research has provided a foundation for a compact vision system for monitoring of a 3D weld pool surface. There are improvements that can be made to apply 3D weld pool monitoring in commercial applications with the compact vision system.

Improvements/Future Work

1. Professionally construct the CVS fixture to ensure component alignment and finer adjustment of laser.
2. Use a laser with a smaller interangle between dots (higher resolution) to allow more dots to be projected onto imaging plane.
3. Fit the camera with a macro lens so the camera can be mounted directly to the CVS fixture. This will allow the CVS fixture to orbit the pipe during welding.
4. Create an embedded system to improve performance of image processing and weld pool reconstruction. Currently, a computer is necessary to monitor the

weld pool surface, but an embedded system could reduce the overall cost and size of a commercial system. Also, the embedded system could be application specific and be designed to monitor a weld pool surface. A field programmable gate array (FPGA) or DSP could handle the entire image processing/weld pool reconstruction algorithms. Since the image is processed in blocks, the image could be processed in parallel with multiple blocks being processed simultaneously. An FPGA system has been developed by researchers to measure discontinuities in the welding process [14]. This idea could be extended for real time monitoring of the 3D weld pool surface in the compact vision system.

5. Add control algorithms to adjust welding parameters in real time to achieve optimal welding as the torch orbits the pipe. This would be the realization of a true real time weld pool control system.

References

1. Song, HongSheng, *Machine Vision Recognition of Three Dimensional Specular Surface for Gas Tungsten Arc Weld Pool*, Ph.D. Dissertation, 2007, University of Kentucky: Lexington, Kentucky.
2. Kanitani, F. et al., *Application of GTAW Welding to Various Products*, Automation and Robotisation in Welding and Allied Processes, 1985: p.195-204.
3. Point Grey Research, <http://www.ptgrey.com/products/flea3>.
4. Coherent Inc, <http://www.coherent.com/Products/index.cfm?1717/Lasiris-SNF-Lasers>.
5. Weglowski, M.S., *Investigation on the Arc Light Spectrum in GTA Welding*, Journal of Achievements in Material and Manufacturing Engineering, 2007, **20**, p.519-522.
6. Knowles, Peter, *Design of Structural Steelwork*, 2nd Edition, Glasgow: Surrey University Press, 1987.
7. Andersen, Kristinn, *Synchronous Weld Pool Oscillation for Monitoring and Control*, IEEE Transactions on Industry Applications, 1997, **33**, p.464-471.
8. Trussel, H.J., Vrhel, M.J., *Fundamentals of Digital Imaging*, 2nd Edition, Cambridge University Press, 2008.
9. Gonzalez, R.C., Woods, R.E., *Digital Image Processing*, 2nd Edition, Prentice Hall, 2002.
10. Hypermedia Image Processing Reference, Department of Artificial Intelligence, University Of Edinburgh, <http://homepages.inf.ed.ac.uk/rbf/HIPR2>.
11. Sandwell, D.T., *Biharmonic Spline Interpolation of GEOS-3 and SEASAT Altimeter Data*, Geophysical Research Letters, 1987, **2**, p.139-141.
12. Zhang, Y.M., Kovacevic, R., Ruan, S., *Sensing and Control of Weld Pool Geometry for Automated GTA Welding*, Transactions of the ASME, May 1995, **117**, p.210-222.
13. Saeed, G., Lou, M., Zhang, Y.M., *Computation of 3D Weld Pool Surface From the Slope Field and Point Tracking of Laser Beams*, Measurement Science and Technology, 2004, **15**, p.389-403.
14. Hurtado, R.H., *FPGA-based Platform Development for Change Detection in GTAW Welding Process*, International Conference on Reconfigurable Computing, 2010, p.61-66.

Vita

Alexander Phillip Maroudis

1. Background
 - a. Born : June 02, 1980
 - b. Place of Birth : Ashland, Kentucky
2. Education
 - a. Bachelors of Science in Electrical Engineering: University of Kentucky, 2003
3. Professional Experience
 - a. ASIC Engineer, Lexmark International, 2003-2009